THE ASTROPHYSICAL JOURNAL, 530:783–799, 2000 February 20
© 2000. The American Astronomical Society. All rights reserved. Printed in U.S.A.

THE *r*-PROCESS–ENRICHED LOW-METALLICITY GIANT HD 115444

JENNY WESTIN,[1,2] CHRISTOPHER SNEDEN,[1] BENGT GUSTAFSSON,[2] AND JOHN J. COWAN[3]
Received 1999 June 30; accepted 1999 October 1

ABSTRACT

New high-resolution, very high signal-to-noise spectra of ultra–metal-poor (UMP) giant stars HD 115444 and HD 122563 have been gathered with the High-Resolution Echelle Spectrometer of the McDonald Observatory 2.7 m telescope. With these spectra, line identification and model atmosphere analyses have been conducted, emphasizing the neutron-capture elements. Twenty elements with $Z > 30$ have been identified in the spectrum of HD 115444. This star is known to have overabundances of the neutron-capture elements, but it has lacked a detailed analysis necessary to compare with nucleosynthesis predictions. The new study features a line-by-line differential abundance comparison of HD 115444 with the bright, well-studied halo giant HD 122563. For HD 115444, the overall metallicity is [Fe/H] $\simeq -3.0$. The abundances of the light and iron-peak elements generally show the same pattern as other UMP stars (e.g., overdeficiencies of manganese and chromium, overabundances of cobalt), but the differential analysis indicates several nucleosynthesis signatures that are unique to each star.

Synthetic spectrum analyses reveal substantial overabundances of the heavier neutron-capture elements ($Z \geq 56$; elements barium and beyond) in HD 115444. Thus with [Eu/Fe] $\simeq +0.9$, for example, HD 115444 is a moderate version of the extremely neutron-capture–rich UMP giant CS 22892−052 ([Fe/H] $\simeq -3.1$, [Eu/Fe] $\simeq +1.7$). The abundance pattern of the heavier neutron-capture elements is consistent with scaled solar system *r*-process–only abundances (with little contribution from the *s*-process). In HD 115444, [Ba/Eu] $= -0.73$, while in CS 22892−052 this ratio is -0.79. Thus HD 115444 becomes the second UMP *r*-process–rich halo giant unambiguously identified from a very detailed abundance analysis. Abundances of the lighter neutron-capture elements strontium, yttrium, and zirconium are, however, nearly identical in HD 115444 and HD 122563.

Along with the heavier neutron-capture elements, the 4019 Å line of Th II has been detected in HD 115444, yielding $\log \varepsilon(\mathrm{Th}) = -2.23 \pm 0.07$. Comparing the observed thorium abundance in HD 115444, along with CS 22892−052, with other theoretical estimates of the time-zero abundance suggests an age for both of these UMP stars of 15.6 ± 4 Gyr, consistent with previous radioactive age estimates for CS 22892−052 and other Galactic and cosmological age determinations.

Subject headings: Galaxy: halo — nuclear reactions, nucleosynthesis, abundances — stars: abundances — stars: Population II

1. INTRODUCTION

The secrets of early Galactic nucleosynthesis are slowly being revealed from the chemical compositions of metal-poor stars. Advances in analytical techniques have been applied to increasing samples of fainter (thus more distant) stars, yielding more sharply defined abundance trends with metallicity for several major element groups. The general abundance patterns (and their exceptions) in stars of the metallicity range $0.0 \geq$ [Fe/H] ≥ -2.5 are now reasonably well established for most spectroscopically accessible elements with atomic numbers $Z \leq 30$.[4] A good recent summary of these trends has been given by Cayrel (1996).

Elements with $Z > 30$, comprising more than half of the periodic table, are synthesized almost exclusively in neutron-capture fusion reactions. Abundance trends with metallicity are on firm ground for relatively few of these neutron-capture elements, primarily because of their small abundances and lack of strong transitions available to ground-based spectroscopy for most of these elements. Nevertheless, some general statements may be made from the extant observations. First, the "bulk" levels of neutron-capture elements vary greatly with respect to the Fe-peak elements in the lowest metallicity stars ([Fe/H] $\lesssim -2.5$), hereafter called ultra–metal-poor (UMP) stars. The neutron-capture–to–Fe ratios can scatter by more than a factor of 100 from star to star at a given metallicity (Gilroy et al. 1988; McWilliam et al. 1995; Burris et al. 1999). Second, the Ba/Eu abundance ratio slowly declines with decreasing metallicity, reaching [Ba/Eu] $\simeq -0.8$ at [Fe/H] $\simeq -3$ (McWilliam 1998; Burris et al. 1999). Europium is synthesized most easily in conditions of extremely high neutron fluxes (during the so-called *r*[*apid*]-process), while barium is most easily made in very low neutron flux environments (during the *s*[*low*]-process). The decline in [Ba/Eu] is thus taken as evidence for the dominance of a Type II supernova–induced *r*-process in producing neutron-capture elements early in the Galaxy's nucleosynthesis history. Third, the abundances of "lighter" Sr–Y–Zr neutron-capture elements ($Z = 38$–40) do not simply scale with those of the "heavier" elements Ba... ($Z \geq 56$). Nor do these lighter neutron-capture elements fit easily into a single nucleosynthesis scheme (e.g., Cowan et al. 1995).

[1] Department of Astronomy and McDonald Observatory, University of Texas, Austin, TX 78712; chris@verdi.as.utexas.edu.

[2] Uppsala Astronomical Observatory, Box 515, S-751 20 Uppsala, Sweden; be@astro.uu.se, bg@astro.uu.se; 94jwe@mail2.tdb.oo.se.

[3] Department of Physics and Astronomy, University of Oklahoma, Norman, OK 73019; cowan@mail.nhn.ou.edu.

[4] We adopt the usual spectroscopic notations that $[\mathrm{A/B}] \equiv \log_{10}(N_\mathrm{A}/N_\mathrm{B})_\mathrm{star} - \log_{10}(N_\mathrm{A}/N_\mathrm{B})_\odot$, and that $\log \varepsilon(\mathrm{A}) \equiv \log_{10}(N_\mathrm{A}/N_\mathrm{H}) + 12.0$, for elements A and B. Also, metallicity will be assumed here to be equivalent to the stellar [Fe/H] value.

Confidence in the *r*-process origin of the heavier neutron-capture elements in UMP stars does not rest solely with the many determinations of [Ba/Eu] ratios, which are still subject to reasonably large observational uncertainties. Instead, the most convincing evidence has come from the detailed abundance distributions of neutron-capture elements in those UMP stars that are bright enough to permit very high resolution, high signal-to-noise spectroscopy (so that very weak neutron-capture element transitions may be detected), or those that have anomalously large neutron-capture/Fe ratios (so that the neutron-capture transitions are detected in high contrast with features of other elements). Such detailed abundance distributions (at least 10 neutron-capture elements) exist for only a few UMP stars. For example, Sneden & Parthasarathy (1983) published a detailed neutron-capture element study of the bright UMP giant HD 122563. These elements are actually underabundant with respect to Fe in HD 122563 (e.g., [Eu/Fe] $\simeq -0.4$). Another UMP giant star, CS 22892−052, originally identified in the objective-prism survey of the halo by Beers, Preston, & Shectman (1985, 1992), is a much fainter star at $V = 13.1$. But it has been the target of several recent abundance studies (Sneden et al. 1994, 1996; Norris, Ryan, & Bees 1997a) because it has the largest overabundances of neutron-capture elements (e.g., [Eu/Fe] $\simeq +1.7$) of any UMP star outside of the CH star domain. The common link between the neutron-capture abundance mixes of HD 122563, CS 22892−052, and many other UMP stars studied by Gilroy et al. (1988) and McWilliam et al. (1995) is the *r*-process signature among the heavy elements. The relative abundance patterns are remarkably similar, and so far are indistinguishable from the abundance pattern of the *r*-process–only parts of solar system material (Käppeler, Beer, & Wisshak 1989; Sneden et al. 1996).

An important aspect of neutron-capture element studies in UMP stars is nucleocosmochronometry. This is the determination of the ages of halo stars (commonly assumed to be nearly equal to the Galactic age) from abundances of elements that radioactively decay with long half-lives. The technique was pioneered by Butcher (1987) and has been applied in practice mainly to the spectroscopically accessible element thorium. This element is synthesized exclusively in the *r*-process and decays with $\tau_{1/2} = 14.0$ Gyr. But the single strong Th II feature routinely available to ground-based spectroscopy is part of a complex atomic and molecular transition blend at 4019 Å, as illustrated in spectra published by Morell, Källander, & Butcher (1992), and François, Spite, & Spite (1993). Thorium abundances accurate enough to be useful for cosmochronometry can be obtained only when [Th/Fe] $\gg 0$, so that the Th II line dominates the other 4019 Å blend components. Stars with high thorium abundances will also have large abundances of other neutron-capture elements. That is fortunate, because determinations of ages from just [Th/Eu] or [Th/Nd] ratios have significant uncertainties due to the big atomic-number gap between thorium and the other elements. A thorium decay age is computed from the difference between the presently observed [Th/neutron-capture] ratio and the estimated value this ratio had immediately after supernova synthesis. Thus, in order to solidify observational aspects of thorium cosmochronometry, many abundances throughout the $Z = 60$–90 range must be determined in many stars. This means that UMP stars with neutron-capture element overabundances must be sought out and subjected to extensive analyses.

The star HD 115444 was first noted in Bond's objective-prism search (Bond 1980) for low-metallicity halo giants. But its unusual spectrum was discovered by Griffin et al. (1982; hereafter GGGV82), who obtained moderately high resolution photographic spectra of HD 115444 after it failed to yield a sensible measurement with Griffin's photoelectric radial velocity spectrometer (Griffin 1967). Their analysis of HD 115444, performed differentially with respect to HD 122563, concluded that HD 115444 probably was more metal-poor than HD 122563 ([Fe/H] $\simeq -3.0$ vs. -2.7). They also found all six neutron-capture elements detected in both stars to be more abundant in HD 115444 than in HD 122563. However, the heaviest neutron-capture elements, Ba, La, and Eu, were far more overabundant than the lighter elements Sr, Y, and Zr. GGGV82 labeled HD 115444 as "a barium star of extreme Population II," but noted that the *r*-process element Eu seemed nearly as overabundant as the *s*-process element Ba. Gilroy et al. (1988) included HD 115444 in their neutron-capture abundance survey of Bond (1980) giants. Their results, determined from an echelle/CCD spectrum, did not indicate an enhancement of barium. Instead, they derived a large europium abundance leading to [Ba/Eu] $\simeq -1.0$, indicative of an *r*-process origin for the heavier neutron-capture elements.

Recently, Sneden et al. (1998a) obtained *Hubble Space Telescope* (*HST*) Goddard High Resolution Spectrograph (GHRS) data in three UV spectral regions of HD 115444, and they detected (for the first time in any UMP star) some transitions of the very heavy neutron-capture elements osmium, platinum, and lead. Unfortunately, their interpretation of the abundances of these elements was somewhat compromised by the uncertain (possibly conflicting) abundances of other neutron-capture elements from the GGGV82 and Gilroy et al. (1988) studies. In this paper our goals are (*a*) to clear up questions on the status of HD 115444 remaining from the earlier ground-based studies; (*b*) to expand the number of detected neutron-capture elements in this unusual star; (*c*) to connect in a consistent way its ground-based and *HST*-based abundances; and (*d*) to make an age estimate for the HD 115444 material from its thorium abundance. We present a comprehensive abundance study of HD 115444 from newly acquired high-resolution, high signal-to-noise spectra spanning the near-UV to red spectral regions. Following the lead of GGGV82, we have analyzed HD 115444 with respect to HD 122563, because the atmospheric parameters of these two halo UMP red giants are so similar. In succeeding sections we describe the data acquisition and reduction, discuss the differential model atmosphere calculations and abundance derivation of these stars, and then concentrate on implications of the neutron-capture element abundances in HD 115444.

2. OBSERVATIONS, REDUCTIONS, AND EQUIVALENT WIDTHS

In 1997 we obtained high-resolution, high signal-to-noise spectra of HD 115444 and HD 122563 with the McDonald Observatory 2.7 m H. J. Smith Telescope and the "2d-coudé" cross-dispersed echelle spectrograph (Tull et al. 1995). Basic data for these two stars are given in Table 1.

TABLE 1

BASIC STELLAR DATA

Quantity	HD 115444	HD 122563
Basic Data		
V[a]	8.96	6.18
$B-V$[a]	0.75	0.85
$U-B$[a]	0.16	0.37
$V-K$[b]	2.34	2.49
$b-y$[c]	0.575	0.640
m_1[c]	0.070	0.095
c_1[c]	0.425	0.520
Spectral type[a]	K0	F8 IV
M_V^d	−0.49	−1.24
M_V^e	−0.8	−1.2
Stellar Model Atmosphere Parameters		
$T_{\rm eff}$	4650	4500
log g	1.50	1.30
[M/H]	−2.90	−2.70
v_t (km s^{-1})	2.1	2.5
[Fe/H]	−2.99	−2.74

[a] Multiple measures taken from SIMBAD database.
[b] K magnitude is from Alonso et al. 1998.
[c] Bond 1980.
[d] Anthony-Twarog & Twarog 1994.
[e] Hanson et al. 1998, rescaled from Bond 1980.

We also obtained companion spectra of a tungsten lamp to use in flat-fielding the raw data frames, a Th-Ar lamp for eventual wavelength calibration of the extracted spectra, and a rapidly rotating hot star for telluric absorption-line cancellation. The spectrograph was configured such that with an entrance aperture width of 1.″2 in the dispersion dimension, the 2 pixel spectral resolving power at the Tektronix 2048 × 2048 CCD was $R \equiv \Delta\lambda/\lambda \simeq 60{,}000$. The spectra spanned the wavelength range 3600 Å $\leq \lambda \leq$ 10000 Å. Blueward of 5900 Å the spectral coverage was complete, but redward of this wavelength the free spectral range of the echelle orders was too large to be contained on the CCD, thus producing wavelength gaps in the recorded spectra. The signal-to-noise (S/N) ratios of the spectra were of course wavelength dependent, such that at 6000 Å, S/N $\simeq$ 500; at 5000 Å, S/N $\simeq$ 400; and at 4000 Å, S/N $\simeq$ 200.

The raw data frames were processed in standard ways using IRAF echelle reduction routines. After extraction of wavelength-calibrated echelle orders, cancellation of telluric spectral features in some of the orders was accomplished with specialized software (Fitzpatrick & Sneden 1987). Sample spectra of HD 115444 and HD 122563 are shown in Figure 1. In general, absorption features in HD 122563 are somewhat stronger than in HD 115444. This makes sense, given previous claims that HD 122563 is more metal-rich and has a lower effective temperature than HD 115444. However, as seen in the upper panel, the transitions of the "heavy" ($Z \geq 56$) neutron-capture elements La and Eu are clearly much stronger in HD 115444. On the other hand, the transitions displayed in the lower panel show no corresponding enhancements of the "lighter" neutron-capture elements Zr and Sr in HD 115444.

Equivalent widths (EWs) were measured in order to derive model atmosphere parameters and to determine abundances for those elements possessing many unblended

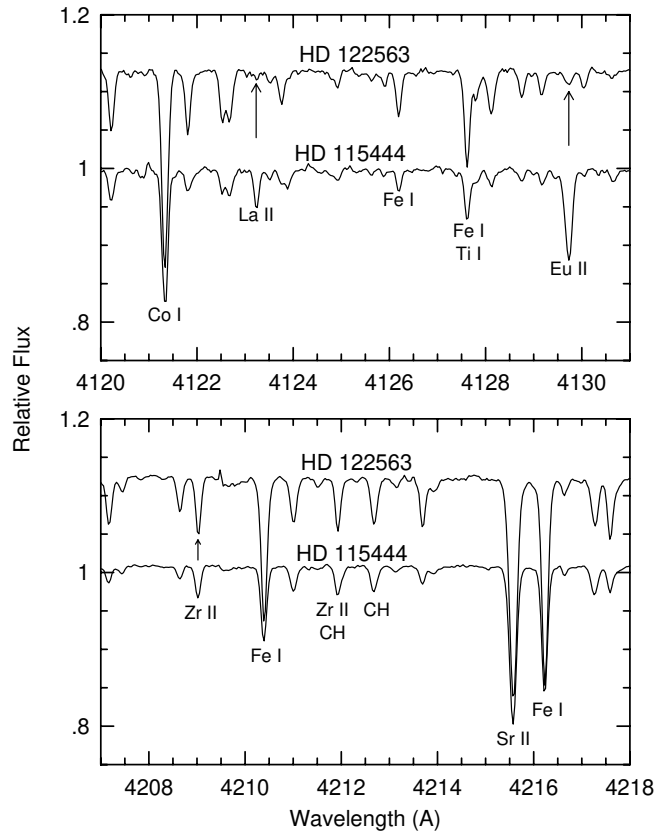

FIG. 1.—Two small spectral regions in HD 115444 and HD 122563. Both panels illustrate the generally stronger lines of HD 122563, caused by its lower $T_{\rm eff}$ and larger metallicity. The top panel shows the much deeper lines of La II and Eu II, hinting at very large overabundances of the heavier neutron-capture elements in this star. But the bottom panel shows that the Zr II and Sr II lines of HD 115444 are actually weaker than those of HD 122563, indicating that the lighter neutron-capture elements have comparable abundance ratios with respect to Fe in both stars.

lines in our spectra. We measured the EWs with the IRAF task SPLOT, using a Gaussian assumption for the line profiles. Two continuum points were marked, and a single best-fit line profile was displayed and examined for obvious blends. Listed in Table 2 are the measured EWs of HD 115444 and HD 122563 together with the excitation potentials (EPs) and transition probabilities (log gf) of the lines. For most lines we adopted the log gf values employed by McWilliam et al. (1995) and Sneden et al. (1996); see those papers for the sources of these data. We also supplemented some log gf values from Fuhr & Wiese (1996). Laboratory gf values have been employed throughout this study; none have been derived from a solar spectral analysis. For those lines that were analyzed using synthetic spectra, the entry "syn" is used in Table 2 instead of an EW value.

We compared our measured EWs with those of previous studies of HD 115444 and HD 122563 in the literature. Taking differences in the sense "this work minus others," the mean differences with the measurements by GGGV82 are for HD 115444, $\langle\delta{\rm EW}\rangle = -15.2 \pm 1.8$ mÅ ($\sigma = 15.9$ mÅ; 79 lines in common); and for HD 122563, $\langle\delta{\rm EW}\rangle = -15.9 \pm 1.8$ mÅ ($\sigma = 16.2$ mÅ; 81 lines). The large line-to-line scatter and the overall offset are undoubtedly due to the use of photographic plates in the 1982 study. Those data had significantly lower S/N and resolution than do the present spectra. On the other hand, Sneden & Parthasarathy's (1983) EWs of HD 122563 agree

TABLE 2

EQUIVALENT WIDTHS

λ	Species	EP	log *gf*	EW 122	EW 115
...	CH	...	...	syn	syn
...	CN	...	...	syn	syn
6300.31.....	O I	0.00	−9.750	syn	syn
8183.30.....	Na I	2.10	+0.260	18	12
8194.84.....	Na I	2.10	+0.559	32	24
3832.31.....	Mg I	2.71	+0.145	230	175
3838.30.....	Mg I	2.72	+0.414	262	190
4571.10.....	Mg I	0.00	−5.569	85	54
4703.00.....	Mg I	4.35	−0.377	72	55
5172.70.....	Mg I	2.71	−0.381	209	175
5183.62.....	Mg I	2.72	−0.158	232	193
5528.42.....	Mg I	4.35	−0.341	78	56
3961.53.....	Al I	0.01	−0.336	146	117
4102.94.....	Si I	1.91	−3.100	84	57
4283.01.....	Ca I	1.89	−0.220	65	45
4318.66.....	Ca I	1.90	−0.210	55	39
4425.44.....	Ca I	1.88	−0.358	50	35
4454.79.....	Ca I	1.90	+0.260	81	66
5349.47.....	Ca I	2.71	−0.310	14	7.5
5581.98.....	Ca I	2.52	−0.555	14	8.5
5588.76.....	Ca I	2.53	+0.358	49	35
5590.13.....	Ca I	2.52	−0.571	12	7.1
5601.29.....	Ca I	2.53	−0.690	15	7.5
5857.46.....	Ca I	2.93	+0.240	26	16
6102.73.....	Ca I	1.88	−0.790	38	23
6122.23.....	Ca I	1.89	−0.320	70	47
6162.18.....	Ca I	1.90	−0.090	84	60

NOTE.—Table 2 is published in its entirety in the electronic edition of The Astrophysical Journal. A portion is shown here for guidance regarding its form and content.

well with our measurements: $\langle \delta \mathrm{EW} \rangle = +0.10 \pm 0.6$ mÅ ($\sigma = 6.2$ mÅ; 108 lines). Gilroy et al. (1988) published data for HD 115444 and HD 122563 as part of a larger survey of stars, and the compared EWs are in reasonable accord: for HD 115444, $\langle \delta \mathrm{EW} \rangle = -4.2 \pm 2.8$ mÅ ($\sigma = 10.9$ mÅ; 15 lines), and for HD 122563, $\langle \delta \mathrm{EW} \rangle = -2.5 \pm 4.4$ mÅ ($\sigma = 12.5$ mÅ; 8 lines). The standard deviations are dominated by a couple of very discrepant lines. Gratton & Sneden (1990) also have a small number of lines in common with our study, but only for HD 122563. Their values agree well with our measurements: $\langle \delta \mathrm{EW} \rangle = +1.3 \pm 1.4$ mÅ ($\sigma = 4.65$ mÅ; 11 lines). Since our new spectra are of higher S/N and resolution than (most of) the compared studies, the encountered differences were not unexpected. On the whole our EWs agree reasonably well with those in the literature.

3. MODEL ATMOSPHERES AND "ORDINARY" ABUNDANCES

3.1. *Derivation of Fundamental Model Parameters*

We first derived stellar model atmospheres and abundances for HD 115444 and HD 122563 in two independent analyses. We then followed the spirit of the GGGV82 study by using HD 122563 as a template star to derive more accurate *differential* model atmosphere parameters for HD 115444. Results of the independent analyses of each star will be labeled "absolute," while the term "relative" will be reserved for results of the differential analysis.

Trial stellar atmosphere models with different values of input parameters ($T_{\rm eff}$, [M/H], log g, and v_t) were generated by a new version of the model atmosphere code MARCS. These atmospheres are one-dimensional, plane-parallel, flux-constant LTE models computed using the opacity sampling scheme with 21,000 wavelength points to approximate the relevant gas opacity properties. MARCS is a modern version of the code described by Gustafsson et al. (1975) and Edvardsson et al. (1993), and it is subject to ongoing refinements. The code, together with the sources of its opacity data, will be described elsewhere. For the current MARCS implementation, modern data for metallic and molecular lines and continua were compiled from many different sources. The mixing-length approximation was used for convection, with parameters $\alpha = \ell/H_p = 1.5$, $\nu = 8$, and $y = 0.076$ (Henyey, Vardya, & Bodenheimer 1965) for our models. An enhancement of 0.4 dex of the α-process elements (from oxygen through calcium) was also assumed.

Final choice among possible trial model atmospheres was made by using them and the measured EWs as input for the current version of the LTE line analysis program MOOG (Sneden 1973). The model parameters were determined as follows.

Effective temperature.—$T_{\rm eff}$ was iteratively adjusted until the trend of Fe I abundance with excitation potential was minimized.

Microturbulence.—v_t mostly affects the abundances derived from strong (saturated) lines. Therefore a plot of abundance versus EW will show a slope if the microturbulence is in error; v_t was iteratively determined by minimizing such slopes.

Gravity.—To find the appropriate log g, we required that the abundance determined from ionized species be equal to the abundance derived from neutral species (Fe and Ti were used).

Metallicity.—The model metallicity was constrained to be close to the derived [Fe/H] value from the Fe line analysis. The model atmosphere parameters for HD 115444 and HD 122563 derived from these criteria are listed in Table 1. The model metallicities, [M/H] = −2.90 for HD 115444 and −2.70 for HD 122563, are both within 0.1 dex of our final [Fe/H] values (−2.99 and −2.74, respectively).

To illustrate the $T_{\rm eff}$ and v_t derivations, Figure 2 shows abundances of Fe I lines derived with the final model of HD 115444 plotted against excitation potential (EP) and the logarithm of the reduced width (log EW/λ). Trends of abundances with EP and log EW/λ have been minimized. The mean Fe I abundances agree to the line-to-line scatter limit ($\sigma \simeq 0.1$ dex) for lines ranging over nearly 5 eV in EP and over 2 orders of magnitude in EW.

In order to investigate internal abundance uncertainties, we computed the dependence of derived abundances for HD 115444 on each of the stellar atmosphere parameters. Relative to the final model, [M/H] was increased by 0.5, $T_{\rm eff}$ by 150 K, log g by 0.3, and v_t by 0.3 km s^{-1}. The abundance changes with these parameter excursions are given in Table 3. Some trends are clear, such as the inevitable rise in all abundances as $T_{\rm eff}$ increases. A metallicity change hardly alters the abundances. Gravity changes affect neutral and ionized species abundances in opposite directions. Larger microturbulence values will decrease the abundances, but this parameter affects just the strong (saturated) lines, and thus is not a large effect for most species in these generally weak-lined stars. Exceptions to this statement are those species exhibiting only saturated lines (e.g., Sr II, Ba II). Even here, the entries of Table 3 constitute a worst-case set of

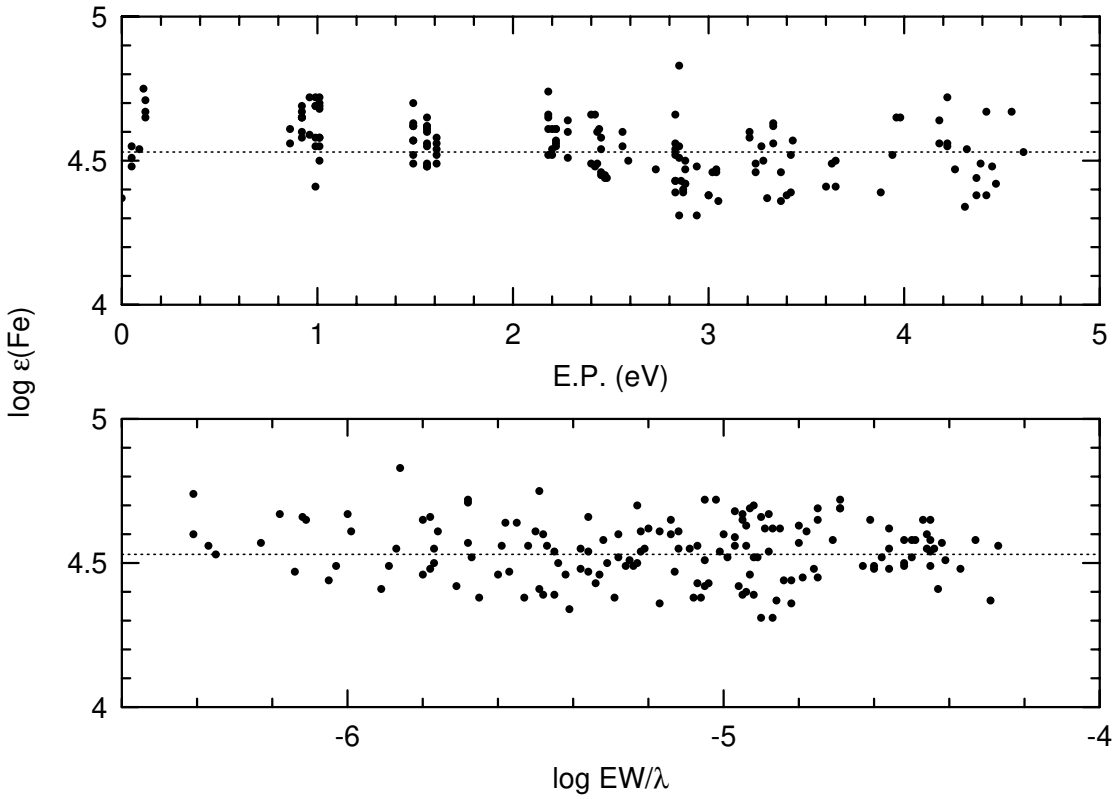

FIG. 2.—Abundances of Fe I lines in HD 115444 plotted as functions of excitation potential (EP) and reduced width (log [EW/λ]). These abundances were generated with the final adopted model for HD 115444.

internal uncertainties. Many *abundance ratios* (i.e., [X/Y] for elements X and Y), will be substantially smaller, especially when comparing abundances from the same ionization states. Furthermore, derivation of $T_{\rm eff}$ and log g through excitation/ionization equilibrium considerations inevitably couples them: higher values of $T_{\rm eff}$ also force higher values of log g, which partially cancels any abundance changes.

The main sources of line-to-line abundance scatter within a species for each star are line blending, log gf uncertainties, and EW measurement errors. These errors can be substantially reduced by computing relative abundances between

TABLE 3

ABUNDANCE DELTAS FOR HD 115444 FOR DIFFERENT MODEL PARAMETERS

Species	δ[M/H] = +0.5	$\delta T_{\rm eff}$ = +150 K	δ log g = +0.5	δv_t (km s^{-1}) = +0.3
Na I	−0.01	+0.08	−0.03	0.00
Mg I	−0.04	+0.15	−0.17	−0.08
Al I	−0.07	+0.13	−0.17	−0.17
Si I	−0.04	+0.15	−0.17	−0.10
Ca I	−0.03	+0.09	−0.06	−0.02
Sc II	+0.01	+0.07	+0.12	−0.03
Ti I	−0.03	+0.02	−0.08	−0.01
Ti II	0.00	+0.06	+0.12	−0.08
V I	−0.03	+0.18	−0.08	0.00
V II	+0.01	+0.06	+0.13	−0.01
Cr I	−0.05	+0.18	−0.10	−0.09
Fe I	−0.03	+0.15	−0.09	−0.06
Fe II	+0.01	+0.01	+0.14	−0.04
Co I	−0.05	+0.16	−0.11	−0.09
Ni I	−0.07	+0.16	−0.13	−0.17
Sr II	−0.02	+0.12	+0.02	−0.27
Y II	+0.01	+0.09	+0.12	−0.05
Zr II	+0.01	+0.08	+0.12	−0.02
Ba II	+0.00	+0.13	+0.11	−0.10
Ce II	+0.01	+0.11	+0.12	−0.01
Nd II	+0.01	+0.12	+0.12	−0.01
Eu II	+0.00	+0.10	+0.10	−0.01
Er II	+0.01	+0.10	+0.10	−0.01

the two stars. We show this in Figure 3 by plotting line-by-line abundance differences $\Delta \log \varepsilon(\mathrm{X}) \equiv \log \varepsilon(\mathrm{X})_{\mathrm{HD}115444} - \log \varepsilon(\mathrm{X})_{\mathrm{HD}122563}$ with respect to EP and EW, using the abundances generated with the final models for each star. Not only are the slopes negligible (implying well-determined T_{eff} and v_t differences), but the line-to-line scatters have shrunk from $\simeq 0.1$ to $\simeq 0.05$ dex. In these relative abundances the uncertainties in individual log gf values have been explicitly eliminated. Additionally, errors due to unaccounted-for line blending should affect the derived abundances in the stars in approximately the same way if the blending agents are transitions of elements with $Z \leq 30$. Thus we expect a further reduction of error in the relative quantities. Some line measurement errors may also be reduced, to the extent that continua have been set and line profiles measured in consistent ways for the two stars. Notice in the lower left-hand panel of Figure 3 that the line-to-line scatter in $\Delta \log \varepsilon$(Fe) is largest for the stronger lines log (EW/$\lambda > -4.8$). These lines lie on the flat and damping portions of the curve of growth, where small EW errors can lead to large abundance errors. But even for these lines the relative Fe abundance is more accurately determined than the absolute abundance of each star.

Choice of model atmosphere code affects the derived stellar parameters and absolute abundance scales. We tested the magnitude of this uncertainty source by deriving atmosphere parameters for the two stars with models interpolated within a recent grid of atmospheres (R. L. Kurucz 1992, private communication) generated with the ATLAS code. The resulting models are approximately 125 K hotter in T_{eff}, about 0.2 dex higher in log g, but require no obvious changes in microturbulent velocities v_t. The derived abundances average $\simeq 0.06$ dex greater with these models. However, model parameter and individual abundance *differences* between the two stars are virtually unchanged by this switch in model codes.

3.2. *External Comparisons*

Our derived model parameters agree well with previous estimates, especially in the differential sense. There are many more published analyses of HD 122563 in the literature than of HD 115444. The most recent "Catalogue of [Fe/H] Determinations" (Cayrel de Strobel et al. 1997) lists 24 spectroscopic analyses of HD 122563. Taking only those analyses based on full model atmosphere calculations, and attempting to eliminate those that adopt most model parameters from other papers, the remaining literature studies on average report $T_{\mathrm{eff}} \simeq 4600$ K, log $g \simeq 1.1$, and [Fe/H] $\simeq -2.65$. The corresponding values from the present study are 4500 K, 1.3, and -2.74. Our derivation of a slightly lower metallicity for HD 122563 probably is a consequence of our lower T_{eff} estimate.

It is more relevant here to discuss those literature studies that treat both of our stars, beginning with effective temperature estimates. Taking differences between the two stars in the sense "HD 115444 minus HD 122563," our temperature analyses yielded $\Delta(T_{\mathrm{eff}}) = 4650 - 4500 = +150$ K. Three spectroscopic studies have dealt with both of these stars. GGGV82 found $\Delta(T_{\mathrm{eff}}) = 4800 - 4600 = +200$ K (and also pointed out that the difference in effective temperatures is more certain than the individual values). Gilroy

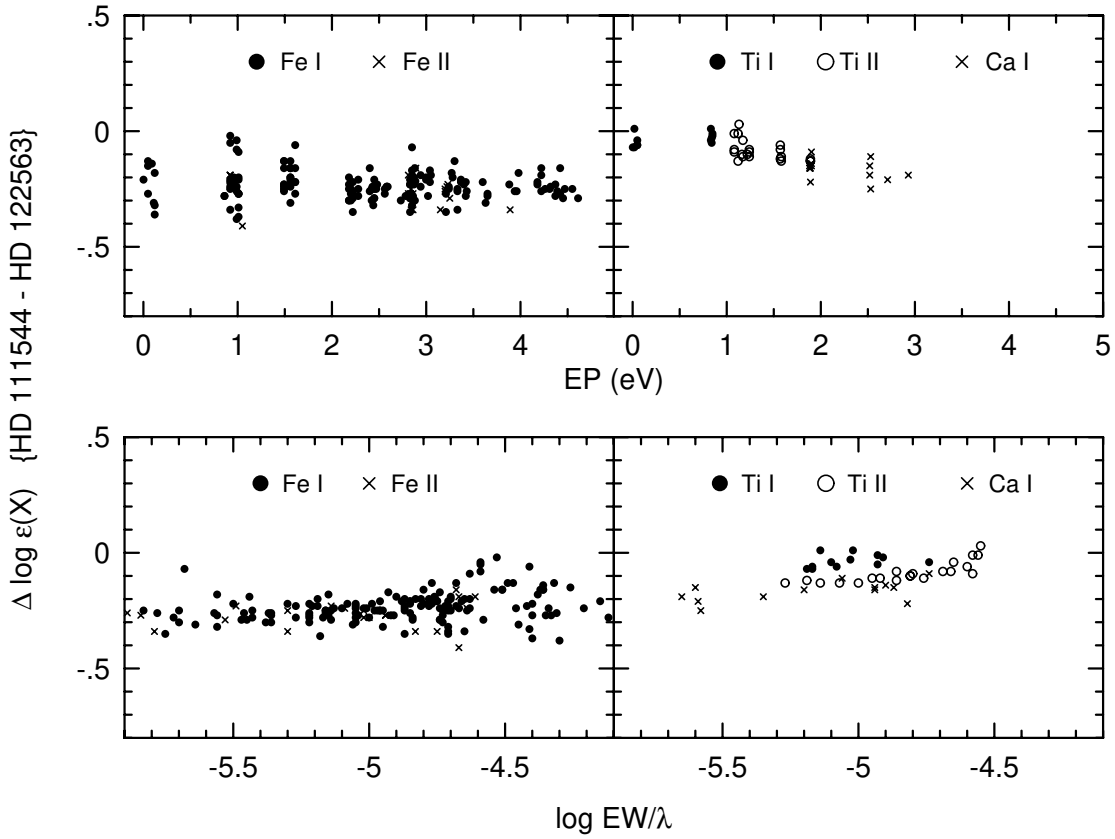

FIG. 3.—Relative abundances between the two stars, of Fe I, Fe II, Ti I, Ti II, and Ca I lines. These abundances were generated with the final adopted models.

et al. (1988) concurred with these values. Gratton & Ortolani (1984) derived $\Delta(T_{\rm eff}) = 4850 - 4680 = +170$ K. Recently, major efforts have been devoted to calibrating broadband photometric indices with $T_{\rm eff}$. The $V-K$ color is nearly a pure function of temperature, and using Di Benedetto's (1998) second-order polynomial fit of $T_{\rm eff}$ to $V-K$ and the colors of Table 1, $\Delta(T_{{\rm eff}V-K}) = 4707 - 4575 = +132$ K. The $B-V$ color is a more complex function of both $T_{\rm eff}$ and [Fe/H], due to the large B-band line blanketing in cool stars. Alonso et al. (1996) derived a relation for $T_{\rm eff}$ in terms of $B-V$ and [Fe/H] variables for main-sequence stars, and A. Alonso (1999, private communicatiion) has provided a similar relation for giant stars. This new formula and the data of Table 1 yield $\Delta(T_{{\rm eff}B-V}) = 4853 - 4717 = +136$ K. None of the spectroscopic or photometric estimates of $T_{\rm eff}$ differences would claim better than $\simeq 50$ K accuracy; thus our newly derived $\Delta(T_{\rm eff}) = +150$ K between the two stars agrees well with the other values. The absolute $T_{\rm eff}$ scale is less certain, and we note that our temperatures are typically ~ 100 K lower than others. This small discrepancy may be partly related to our use of MARCS model atmospheres (§ 3.1). But it does not affect any of the basic conclusions of this paper and will not be considered further here.

The derived gravity difference is $\Delta(\log g) = 1.50–1.30 = +0.20$. Similar results were obtained by GGGV82, $\Delta(\log g) = 1.6–1.2 = +0.4$, and by Gratton & Ortolani (1984), $\Delta(\log g) = 1.60–1.50 = +0.10$. The gravity difference derived by Gilroy et al. (1988) is somewhat larger, $\Delta(\log g) = 2.0–1.2 = +0.8$, but the agreement among the other studies indicates that the Gilroy et al. $\log g$ value for HD 115444 is probably too large.

Our estimation of the microturbulence difference is $\Delta(v_t) = 2.1–2.5 = -0.4$ km s^{-1}. Previous results for the microturbulence vary. GGGV82 found the same value in both stars, $v_t = 2.6$ km s^{-1}, as did Gratton & Ortolani (1984), $v_t = 3.0$ km s^{-1}. Gilroy et al. (1988) derived $\Delta(v_t) = 2.2–2.3 = -0.1$ km s^{-1}. These comparisons are not very enlightening, but do suggest that the microturbulence values for the two stars are not very different.

We determined a relative metallicity $\Delta \log \varepsilon({\rm Fe}) = -2.99$ to $-2.74 = -0.25$ (and -0.24 from the line-by-line differential analysis), taking the mean of neutral and ionized species (Table 4). This difference is not easily anticipated by past spectroscopic studies. Previously estimated [Fe/H] metallicities for HD 115444 and HD 122563 are -2.95 and -2.75, respectively (GGGV82); -2.0 and -2.0 (Gratton & Ortolani 1984); -2.5 and -2.6 (Gilroy et al. 1988). These literature metallicity values bear little relationship to the microturbulent velocities determined in each study, and the analysis techniques are dissimilar enough to not warrant further exposition here. Some calibrated photometric indices provide further estimates of the metallicities: [Fe/H] $= -2.7$ for HD 115444 and -2.6 for HD 122563 (Bond 1980, *uvby*); -2.56 and -2.47 (Anthony-Twarog & Twarog 1994, *uvby*); -2.83 and -2.58 (Clariá et al. 1994, DDO δ4548). Thus, taken as a whole, the previous spectroscopic and photometric investigations do not disagree with the modest metallicity difference found in the present work.

We performed a further check on the spectroscopically derived gravity, by computing an "evolutionary" gravity using the standard formula

$$\log g_{\rm evol} = -12.50 + 0.4(M_V + {\rm BC}) + \log \mathscr{M} + 4 \log T_{\rm eff},$$

which combines Newton's gravitation law with the Stefan-Boltzmann law, eliminating the stellar radius R. We assumed masses equal to the standard mass of stars near the Population II turnoff, $\mathscr{M} = 0.85\, \mathscr{M}_\odot$. With the derived $T_{\rm eff}$ values, we used the calibrations of Montegriffo et al. (1998) to determine bolometric corrections BC $= -0.50$ for HD 115444 and -0.59 for HD 122563. There are a few photometric estimates of M_V for the two stars in the literature. Anthony-Twarog & Twarog (1994) derived for HD 115444 and $M_V = -1.24 \pm 0.4$ for HD 122563, while Hanson et al. (1998) suggest $M_V = -0.8 \pm 0.5$ and $M_V = -1.2 \pm 0.5$ (from a renormalization of the M_V estimates of Bond 1980). Using the Anthony-Twarog & Twarog absolute magnitudes in the above equation yield $\log g_{\rm evol} = 1.70 \pm 0.20$ for HD 115444 and $\log g_{\rm evol} = 1.31 \pm 0.20$ for HD 122563, and the Hanson et al. magnitudes yield $\log g_{\rm evol} = 1.6 \pm 0.2$ and $\log g_{\rm evol} = 1.3 \pm 0.2$, respectively. This is in good agreement with our $\log g$ estimates.

Hipparcos parallaxes (ESA 1997) exist for both stars: 3.55 ± 1.12 milliarcsec for HD 115444 and 3.76 ± 0.72 milliarcsec for HD 122563—almost the same values. But the apparent V of HD 122563 is 2.78 mag smaller than that of HD 115444. The standard distance modulus relation ($M_V = V + 5 \log p + 5 - A_V$) then implies nearly the same difference in absolute magnitudes in the absence of significant interstellar medium (ISM) extinction. This is surprising, since these stars, both red giants with very similar derived atmosphere parameters, would be expected to differ little in luminosity (as they indeed do according to literature estimates). Using the evolutionary gravity equation for HD 122563, and adopting Bond's (1980) estimate that $A_V = 0.0$, we calculated from the *Hipparcos* parallax that $\log g_{\rm Hipp} = 1.42 \pm 0.21$, very close to our spectroscopic $\log g = 1.30$. The uncertainty in $\log g_{\rm Hipp}$ was computed from the maximum and minimum values permitted by the uncertainties in the quantities upon which it depends. Repeating the same calculation for HD 115444 (for which Bond also estimated $A_V = 0.0$) gave $\log g_{\rm Hipp} = 2.58 \pm 0.33$; this is far from our estimate (in agreement with others) of $\log g = 1.50$. From this discussion and the results of literature comparisons, probable statistical biases make it very risky to use such small parallaxes with large relative errors (34% for HD 115444).

3.3. *Light and Iron-Peak Elements*

With the final model atmospheres, we determined abundances for nearly all elements with $Z \leq 30$ from their measured EWs. The exception was manganese, for which we treated the strong Mn I lines in synthetic spectrum calculations, obtaining the hyperfine substructure components from Kurucz's (1999) web site. Mean $\log \varepsilon$(X) abundances and [X/Fe] relative abundance ratios are given for both stars in Table 4. For a species with at least three available transitions in a stellar spectrum, the standard deviation of the sample σ quoted in Table 4 is simply the internal scatter of individual measurements. The mean of those values is $\langle \sigma \rangle = 0.10$ for HD 115444 (24 measures), and 0.12 for HD 122563 (15 measures). We take the average of these numbers as representative of the scatter of individual values of a given abundance for our stars. Thus for a species with only one transition we entered 0.11 as σ in Table 4, and for a species with two transitions we entered the greater of 0.11 and the measured σ. In subsequent discussions we will use these σ-values for the abundance uncertainties, rather than

TABLE 4

ABUNDANCES FOR HD 115444 AND HD 122563

	HD 115444				HD 122563				DIFFERENCE[a]	
SPECIES	log ϵ	σ	Number	[X/Fe]	log ϵ	σ	Number	[X/Fe]	Δ(log ϵ)	σ
C I	+5.46	0.11	...	−0.11	+5.36	0.11	...	−0.46	+0.10	0.06
N I	+6.30	0.11	...	+1.24	+6.40	0.11	...	+1.09	−0.10	0.06
O I	+6.60	0.11	1	+0.66	+6.80	0.11	1	+0.61	−0.20	0.06
Na I.....	+3.34	0.11	2	0.00	+3.44	0.11	2	−0.15	−0.10	0.06
Mg I	+5.13	0.12	7	+0.54	+5.35	0.12	7	+0.51	−0.22	0.12
Al I.....	+3.12	0.11	1	−0.36	+3.41	0.11	1	−0.32	−0.29	0.06
Si I	+5.02	0.11	1	+0.46	+5.27	0.11	1	+0.46	−0.25	0.06
Ca I	+3.75	0.06	13	+0.38	+3.91	0.09	13	+0.29	−0.17	0.04
Sc II	+0.28	0.05	5	+0.17	+0.51	0.08	5	+0.15	−0.23	0.06
Ti I.....	+2.40	0.06	12	+0.40	+2.44	0.07	12	+0.19	−0.04	0.03
Ti II	+2.45	0.13	21	+0.45	+2.53	0.15	21	+0.28	−0.09	0.05
V I	+1.14	0.20	2	+0.13	+1.33	0.11	2	+0.07	−0.19	0.06
V II.....	+1.16	0.11	2	+0.15	+1.40	0.11	2	+0.14	−0.24	0.06
Cr I	+2.40	0.13	6	−0.28	+2.54	0.15	6	−0.39	−0.14	0.03
Mn I	+1.90	0.16	6	−0.50	+2.39	0.19	6	−0.26	−0.49	0.04
Fe I	+4.54	0.10	158	+0.01	+4.78	0.12	158	0.00	−0.23	0.06
Fe II.....	+4.52	0.07	23	−0.01	+4.78	0.10	23	0.00	−0.26	0.05
Co I.....	+2.24	0.10	4	+0.31	+2.50	0.20	4	+0.32	−0.26	0.10
Ni I	+3.25	0.03	3	−0.01	+3.55	0.05	3	+0.04	−0.30	0.05
Cu I.....	+0.53	0.11	1	−0.69	+0.72	0.11	1	−0.75	−0.19	0.06
Zn I.....	+1.86	0.11	2	+0.25	+2.06	0.11	2	+0.20	−0.20	0.06
Ge I.....	−0.05	0.11	1	−0.47	−0.03	0.11	1	−0.70	−0.02	0.06
Sr II	+0.23	0.11	2	+0.32	+0.33	0.11	2	+0.17	−0.10	0.06
Y II.....	−0.82	0.12	8	−0.07	−0.75	0.11	8	−0.25	−0.07	0.04
Zr II.....	−0.02	0.12	5	+0.37	+0.04	0.19	5	+0.18	−0.05	0.09
Ba II	−0.68	0.09	4	+0.18	−1.54	0.13	4	−0.93	+0.85	0.21
La II	−1.40	0.10	5	+0.37	−2.22	0.11	2	−0.70	+0.85	0.06
Ce II	−1.10	0.12	5	+0.34	−1.92	0.11	1	−0.73	+0.82	0.06
Pr II.....	−1.82	0.34	3	+0.46	...	...	...	...	...	...
Nd II.....	−0.93	0.12	10	+0.56	−1.54	0.11	2	−0.30	+0.72	0.12
Sm II.....	−1.18	0.16	4	+0.81	...	...	...	...	...	...
Eu II	−1.63	0.07	5	+0.85	−2.59	0.11	2	−0.36	+1.01	0.06
Gd II.....	−0.98	0.13	3	+0.89	...	...	...	...	...	...
Dy II	−1.01	0.10	5	+0.88	...	...	...	...	...	...
Ho II.....	−1.85	0.11	2	+0.64	...	...	...	...	...	...
Er II.....	−1.21	0.02	3	+0.85	−2.27	0.11	2	−0.46	+1.07	0.06
Tm II.....	−1.79	0.11	1	+1.07	...	...	...	...	...	...
Yb II	−1.40	0.11	1	+0.51	−2.62	0.11	1	−0.96	+1.22	0.06
Os I	−0.55	0.11	1	+0.99	...	...	...	...	...	...
Pt I.....	−0.30	0.11	1	+0.89	...	...	...	...	...	...
Th II	−2.23	0.11	1	+0.64	...	...	...	...	...	...
U II	<-2.6	...	1	$<+0.5$	...	...	...	...	...	...

[a] The difference $\Delta \log \epsilon \equiv \log \epsilon$(HD 115444) − $\log \epsilon$(HD 122563).

the more commonly employed standard deviations of the means [σ/(number of lines)$^{1/2}$]. Adoption of the more conservative σ allows many remaining uncertainties of scale (from choices of model atmosphere grids, transition probabilities, etc.) to be effectively accounted for. These σ's are also far more realistic abundance uncertainty estimates for species with small numbers of measured transitions.

In Figure 4 we show the individual abundances [M/H] for all the elements. The horizontal solid line at [M/H] = −2.99 in this figure represents the mean [Fe/H] for HD 115444, and the horizontal dotted line at [M/H] = −2.74 is the mean [Fe/H] for HD 122563. For clarity in this figure the abundance σ's from Table 4 are not plotted, but of course they should be remembered when the abundances of different elements are compared. The data of Table 4 and Figure 4 demonstrate that the light and Fe-peak abundances (elements with $Z \leq 30$ shown in the upper panel) in HD 115444 and HD 122563 generally follow the abundance patterns of UMP stars (e.g., McWilliam et al. 1995; Ryan, Norris, & Beers 1996; Cayrel 1996). That is, O, Mg, Si, and Ti are enhanced relative to iron, while Al, Cr, Mn, and Cu are all deficient. In fact, nearly all of these abundance ratios of our program stars are within 0.1 dex of the mean ratios summarized in Cayrel's Figure 4.

However, some noteworthy anomalies exist in the abundance patterns. To see this more clearly, in Table 4 we also give for all species the abundance differences between the two stars. These differences, like those discussed in § 3.1, were computed on a line-by-line basis. As before, we define $\Delta \log \varepsilon(\mathrm{X}) \equiv \log \varepsilon(\mathrm{X})_{\mathrm{HD}115444} - \log \varepsilon(\mathrm{X})_{\mathrm{HD}122563}$. The single-measure standard deviation in the relative abundance $\sigma(\Delta \log \varepsilon(\mathrm{X}))$ is usually much smaller than those of the absolute abundances $\sigma(\log \varepsilon(\mathrm{X}))$. For species with three or more transitions, $\langle \sigma(\Delta \log \varepsilon(\mathrm{X})) \rangle = 0.06 \pm 0.01$ from 13

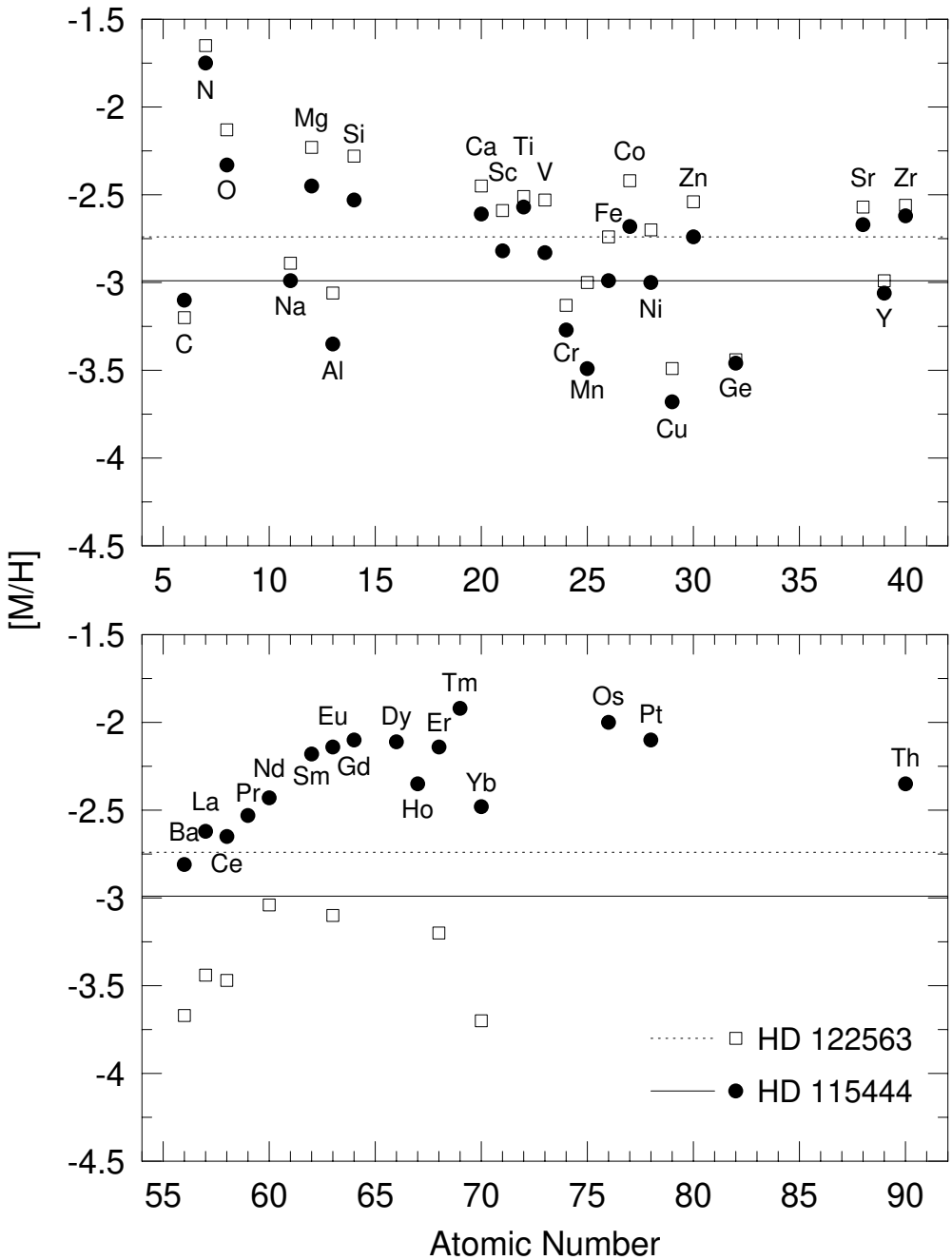

FIG. 4.—Individual abundances for HD 115444 and HD 122563. The upper panel shows the abundances for the light and Fe-peak elements and the lightest neutron-capture elements, and the bottom panel shows the abundances of the heavier neutron-capture elements. The solid horizontal line at [Fe/H] = −2.74 represents the metallicity of HD 122563, and the dotted horizontal line at [Fe/H] = −2.99 represents the metallicity of HD 115444. Element symbols are plotted at the appropriate atomic number and most convenient [M/H] position near a data point.

values, excluding the anomalously large scatter in Ba II. Therefore 0.06 is entered as $\sigma(\Delta \log \varepsilon(X))$ for a species with only one transition, and the greater of 0.06 and the measured value is entered for a species with two transitions.

The abundance differences from Table 4 are displayed in Figure 5 (not every element was detected in HD 122563). For the elements with detected transitions of both neutral and ionized species (Ti, V, and Fe), we plot a single point representing the mean differences. The vast majority of elements with $Z \leq 30$ (13 out of 18) have $\Delta \log \varepsilon(X)$ values within 2 σ of $\Delta \log \varepsilon(Fe) = -0.24$. The abundances of these elements thus simply scale with the metallicity difference between the two stars. The most notable exceptions are the large relative C, Ti excesses and the significant relative Mn underabundance in HD 115444. For elements with $Z > 30$ our results, supporting and extending those of GGGV82 and Gilroy et al. (1982), show only a small enhancement of the lighter neutron-capture elements in HD 115444 but about a factor of 10 difference among the heavier elements. We will now comment on these and other individual abundances:

The CNO *group: carbon.*—The CNO elements were not of primary interest in this study, so to determine carbon and nitrogen abundances we simply adopted the atomic and molecular line lists from the Kurucz (1999) web site for synthetic spectrum analysis of selected portions of the CH

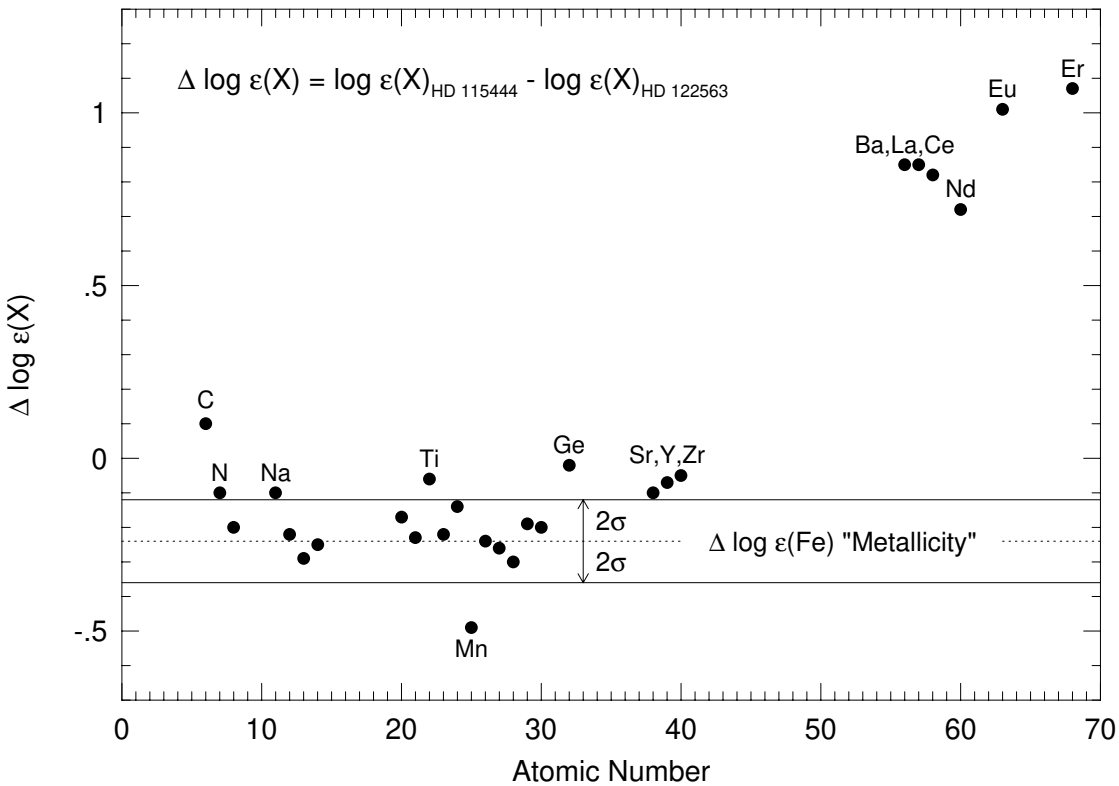

FIG. 5.—Differential abundances for HD 115444 and HD 122563. The definition of $\Delta \log \varepsilon(X)$ identical to that of Fig. 3. The horizontal dashed line is placed at $\Delta \log \varepsilon(Fe) = -0.24$, and solid horizontal lines are drawn at $\Delta \log \varepsilon(X) = -0.12$ and -0.36, representing $\pm 2\,\sigma$ excursions from $\Delta \log \varepsilon(Fe)$. See the text for further discussion of these points.

$A\ ^2\Delta$–$X\ ^2\Pi$ G band and the CN $B\ ^2\Sigma^+$–$X\ ^2\Sigma^+$ violet bands. With these line lists we derived a clear abundance enhancement of C in HD 115444 relative to HD 122563 (Table 4, Fig. 5). This agrees with the initial findings of GGGV82, who suggested that [C/Fe] $\simeq 0$ in HD 115444, while [C/Fe] $\simeq 0.4$ in HD 122563. Furthermore, although the [C/Fe] estimates of Kraft et al. (1982) are nearly identical for these two stars, so are their [Fe/H] estimates. If we translate their and our abundances to [C/H] values, we agree that [C/H] $= -3.1$ and -3.2 for HD 115444 and HD 122563, respectively. Finally, both Sneden (1973) and Norris et al. (1997a) also derived [C/H] $= -3.1$ for HD 122563. All the analyses for C are in agreement.

The CNO *group: nitrogen.*—The only detectable CN violet absorption in these stars occurs at the (0, 0) vibrational bandhead at 3883 Å. From the synthetic/observed spectrum comparisons we estimate [N/Fe] $\simeq +1.2$ for HD 115444 and $+1.1$ for HD 122563, or [N/H] $\simeq -1.8$ and -1.7, respectively. The estimated abundance uncertainty in fitting the very weak CN bandhead is $\simeq \pm 0.25$ dex. The Kraft et al. (1982) nitrogen abundances are somewhat smaller, [N/H] $\simeq -2.3$ and -2.2. Sneden (1973) obtained a larger abundance for HD 122563, [N/H] $\simeq -1.5$, while the Norris et al. (1997a) value for this star is nearly identical to ours. A renormalization probably needs to be applied to either the Kraft et al. N abundances or to the other studies (or maybe to both sets of N abundances). Resolution of this question is beyond the scope of our work. A substantial improvement would be the observation of the NH $A\ ^3\Pi_i$–$X\ ^3\Sigma^-$ bands near 3360 Å. But the relative N abundance between the two stars is likely to remain quite small in future analyses.

The CNO *group: oxygen.*—For the oxygen abundance determination we used the [O I] line at 6300.3 Å. This line and the much weaker [O I] λ6363 line are the usual oxygen abundance transitions of choice for red giants. We derived [O/Fe] $= +0.66$ for HD 115444, and [O/Fe] $= +0.61$ for HD 122563. The latter value is in excellent agreement with the early work on HD 122563 by Lambert, Sneden, & Ries (1974): [O/Fe] $= +0.6$.

Other light elements.—The "pure" α-capture elements Mg, Si, and Ca have nearly identical normal UMP star overabundances in both stars. But caution should be exercised in interpreting the Si abundance, as it is based on only one strong Si I line at 4102.94 Å. Another potentially useful Si I line at 3905.53 Å is severely blended by CH λ3905.67; the higher excitation Si I lines in the yellow-red were undetectably weak on our spectra. The Al abundance rests solely on the Al I λ3961.53 resonance line, as its companion at 3944 Å suffers CH blending (Arpigny & Magain 1983). The derived Al underabundances in both stars, [Al/Fe] $= -0.36$ for HD 115444 and -0.29 for HD 122563, are, however, in good agreement with other values for UMP stars (Cayrel 1996). The Na abundance is based on the Na I doublet $\lambda\lambda$8183.2, 8194.8, which occurs amid a thicket of telluric H_2O lines. Our EWs for the Na I lines may not be as reliable as most other transitions. But the present [Na/Fe] $= 0.00$ for HD 115444 and -0.15 for HD 122563 are in good agreement with those derived by Pilachowski, Sneden, & Kraft (1996): $+0.04$ and -0.05, respectively. The Pilachowski et al. abundances were based on spectrum syntheses of the $\lambda\lambda$5682.6, 5688.2 doublet, and give no indication that our Na abundances from the longer wavelength lines are in error.

Iron-peak elements.—The Fe-peak abundance pattern in our stars (Fig. 4) follows the general distribution in other UMP stars, and HD 115444 generally cannot be distinguished from HD 122563. A conspicuous exception to this statement is manganese, for which we derive very different abundances in the two stars: $\Delta \log \varepsilon(\mathrm{Mn}) = -0.49$, more than 4 σ smaller than $\Delta \log \varepsilon(\mathrm{Fe})$. The Mn anomaly is easily seen from inspection of the data: whereas typical weak Fe-peak absorption features in the HD 115444 spectrum are about half as strong as those in the HD 122563 spectrum, the weak Mn I lines are a third as strong (Table 2). The Mn result is not an artifact of neglect of hyperfine splitting in the analyses, as we performed spectrum syntheses with the full hyperfine substructure for the strong $\lambda\lambda$4030.7, 4033.0, 4034.4 lines. The relative Mn abundance difference between these two stars therefore seems to be real. A future check on this result ought to be the observation of Mn II lines in the 3400 Å spectral region. For copper there are extreme deficiencies in both stars ([Cu/Fe] $\simeq -0.7$), but this is not a new result; all UMP stars apparently have very depressed levels of copper (Sneden, Gratton, & Crocker 1991).

Titanium (probably belonging to both α-capture and Fe-peak element groups) is overabundant, but much more so in HD 115444; the mean of Ti I and Ti II relative abundances is $\Delta \log \varepsilon(\mathrm{Ti}) = -0.06$, which is about 3 σ higher than $\Delta \log \varepsilon(\mathrm{Fe})$. As with the case of Mn, the Ti anomaly can be readily forecast by inspection of the spectra of the two stars. The Ti abundance difference is not easily explained, as it is based on large numbers of both neutral and ionized species transitions. Departures from LTE, which are conceivable as such, probably cannot account for this abundance difference, since we must demand that any proposed non-LTE corrections should affect neutral and ionized species abundances in significantly different ways in the two stars.

3.4. *The Neutron-Capture Elements*

The abundances of the neutron-capture elements ($Z > 30$) were determined by EWs or by synthetic spectra, as indicated in Table 2. The line lists for these calculations were those originally developed for the abundance analysis of CS 22892−052 (Sneden et al. 1996). Hyperfine structure was explicitly accounted for in the abundance computations for Ba, La, and Eu; see Sneden et al. for further discussion and references to the laboratory data. An example of a synthetic spectrum fitted to the same features in both stars is shown in Figure 6. It is clear that the derived abundance from the Eu II feature in HD 115444 is greatly enhanced relative to that in HD 122563. As HD 115444 is more metal-poor than HD 122563, the contrast in the europium abundance is very large between the two stars. This statement holds for all of the heavier ($Z \geq 56$) elements (Table 4 and Fig. 5). On the other hand, the lighter neutron-capture elements ($32 \leq Z \leq 40$) are only weakly enhanced in HD 115444. These results were anticipated from the spectra presented in Figure 1 and are in qualitative agreement with the earlier studies of GGGV82 and Gilroy et al. (1988).

With this work we have increased to 20 the total number of neutron-capture element abundances in HD 115444. The reader is reminded that the abundances for Ge, Os, and Pt were obtained from comparing extant *HST* GHRS observations in three small UV spectral intervals to synthetic spectrum computations with the newly derived models. As

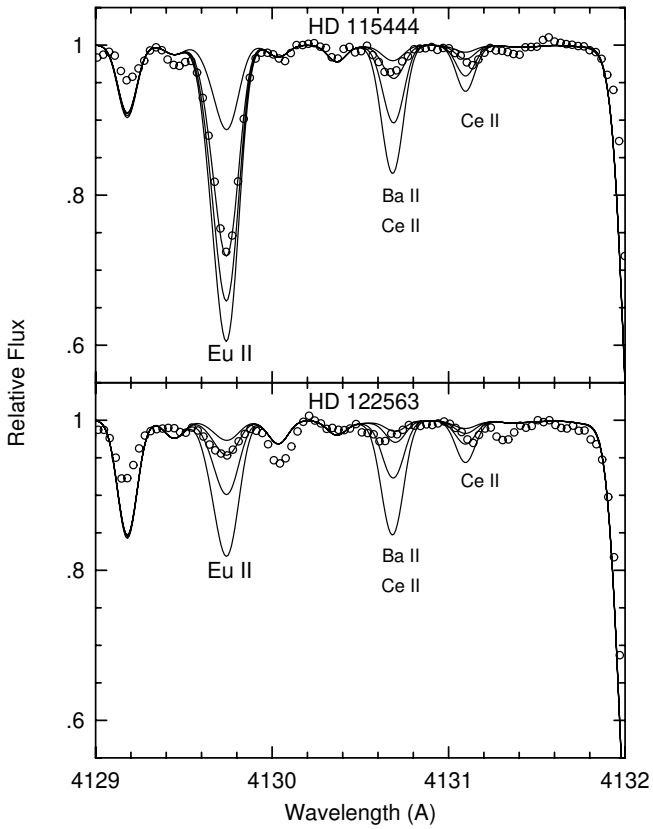

FIG. 6.—Synthetic and observed spectra of the Eu II λ4129.8 line and other nearby neutron-capture features. The observed data points are represented by open circles. For HD 115444 (*top panel*), synthetic spectra have been generated for log ε(Eu) = −2.39, −1.61, −1.39, and −0.99, while for HD 122563 (*bottom panel*) the synthetic spectra are for log ε(Eu) = −2.99, −2.64, −2.19, and −1.89.

expected, the new abundances do not differ significantly from those of Sneden et al. (1998a), because the new model parameters are not significantly different from the ones used in that study (the new models are about 100 K cooler in T_{eff} and about 0.15 dex lower in log g). Sneden et al. urged caution in interpretation of their lead abundance, which was derived from one weak Pb I line (possibly corrupted by a noise spike) at 2833.05 Å. Our new inspection of that line reaffirmed the earlier concerns, and so we decided not to include Pb among the neutron-capture elements in our present work.

3.5. *Thorium and Uranium*

The Th II 4019.1 Å line is the only thorium feature that has been employed for abundance determination in metal-poor stars, although recently Sneden et al. (1998b) have detected the weaker 4086.5 Å line in the extremely *r*-process–rich star CS 22892−052. The 4019 Å line is heavily blended, and several previous studies (e.g., Morell et al. 1992; François et al. 1993; Norris et al. 1997b) have carefully considered possible contaminant lines to the total feature. A preliminary Th abundance in HD 115444 has been presented by Cowan et al. (1999a) from a spectrum combined from our 2d-coudé data and similar data from the Keck I HIRES. Here we discuss the analysis of just the 2d-coudé data.

We carried out synthetic spectrum computations for both stars, varying several elemental and CH abundances in

order to get the best overall match to the observed feature. In Figure 7 we show the results of these experiments. In each panel, syntheses with different thorium abundances are displayed. The solid line represents the case where Th is deleted from the analyses. To set the strengths of the ^{13}CH lines, we first determined carbon isotope ratios from synthetic spectra of the $A\ ^2\Delta$–$X\ ^2\Pi$ band lines near 4230 and 4370 Å, obtaining $^{12}C/^{13}C = 4.0 \pm 1.5$ for HD 122563 and 6.0 ± 1.5 for HD 115444 (in agreement with earlier studies by Lambert & Sneden 1977 and Sneden, Pilachowski, & VandenBerg 1986). Then we empirically determined the CH abundance that would best match the observed ^{12}CH $B\ ^2\Sigma$–$X\ ^2\Pi$ lines surrounding 4019 Å (for example, the $\lambda\lambda$4020.0, 4020.2 CH pair shown in Fig. 7). Finally, the strengths of the ^{13}CH $\lambda\lambda$4018.97, 4019.14 lines were scaled down by the $^{12}C/^{13}C$ ratio.

For HD 122563 the entire 4019 Å absorption may be satisfied without any contribution from the Th II line (Fig. 7, *bottom panel*). We can only suggest that $\log \varepsilon(\mathrm{Th}) \lesssim -3.1$ in this star. The lack of Th detection is, however, consistent with the low abundances of all other neutron-capture elements in HD 122563. The Th II line is cleanly detected in HD 115444; it dominates the rest of the absorption near 4019.1 Å (Fig. 7, *top panel*). The best-fit synthetic spectrum yields $\log \varepsilon(\mathrm{Th}) = -2.23 \pm 0.05$, where the quoted error is a measure of uncertainty in the fitting procedure. This value is to be preferred to the preliminary values estimated by Cowan et al. (1999a) of $\log \varepsilon(\mathrm{Th}) = -2.10 \pm 0.1$. Cowan *et al.* also unsuccessfully tried to detect the 4086 Å Th II line. We concur here with their assessment that from this feature, $\log \varepsilon(\mathrm{Th}) \leq -2.2$, not inconsistent with the detected 4019 Å line.

Cowan et al. (1999a) also employed their combined spectrum to search for features of uranium in HD 115444. The most promising line of U II occurs at 3859.58 Å, but in most cool stars it is hopelessly lost amid the strong CN absorption in this spectral region. But since CN is extremely weak in HD 115444, a search for this line is feasible. However, Cowan et al., and now we, fail to detect the line (see their Fig. 6), and the upper limit we derive from the 2d-coudé spectrum is $\log \varepsilon(\mathrm{U}) < -2.6$. All other U II lines in the visible and near-UV spectral lines should be undetectably weak in HD 115444.

4. DISCUSSION

Our abundance analyses have indicated the following: (1) The heavier neutron-capture elements are overabundant by a factor of 10 in HD 115444 compared to HD 122563. (2) The iron-peak elements have similar abundances in HD 122563 and HD 115444, with the notable exceptions of Ti and Mn. (3) The carbon abundance is high in HD 115444. We discuss these points in more detail in this section.

4.1. *Comments on the* CNO *Abundances*

Nearly all high-luminosity ($M_V \lesssim 0$) halo giant stars exhibit very low $^{12}C/^{13}C$ ratios and low total carbon abundances, indicating efficient operation of CN-cycle nucleosynthesis and convective envelope dredge-up along the giant branch. The required envelope mixing is much more

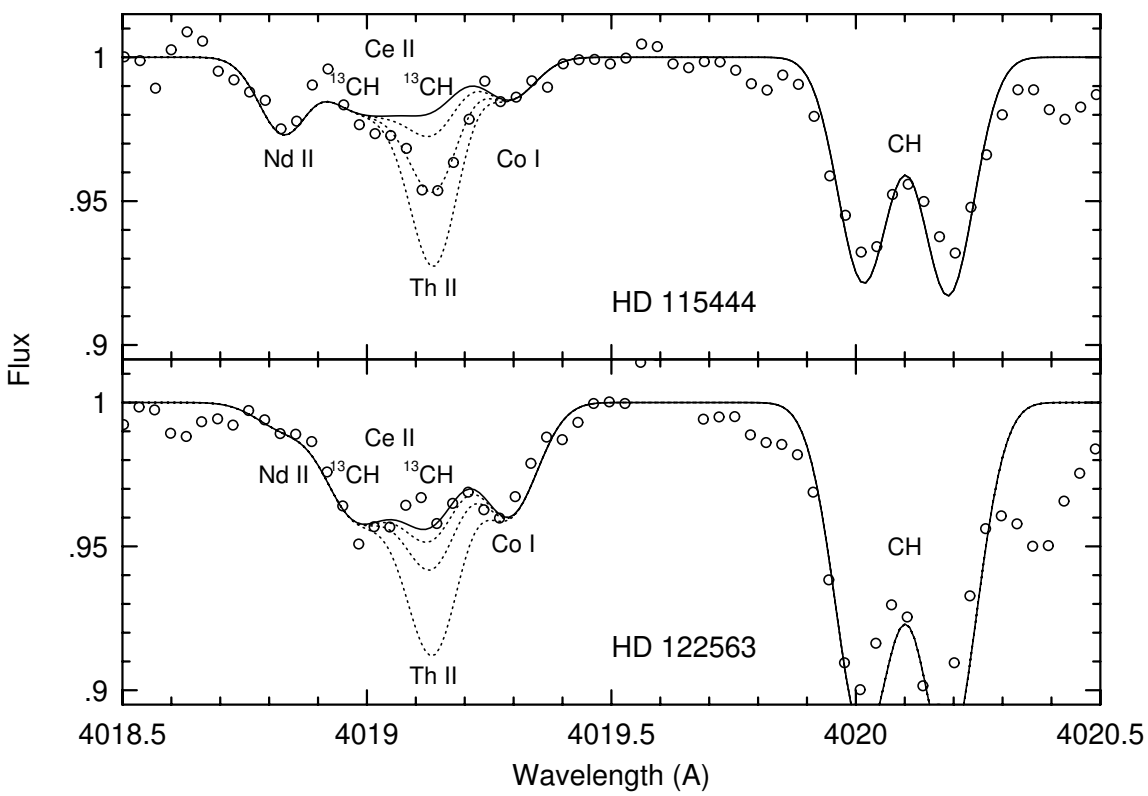

FIG. 7.—Synthetic and observed spectra of the Th II λ4019.1 line and associated contaminant features. The observed data points are represented by open circles. The main blending species transitions have been labeled. For HD 115444 (*top panel*), synthetic spectra have been generated for $\log \varepsilon(\mathrm{Th}) = -\infty$, -2.48, -2.23, and -1.98, while for HD 122563 (*bottom panel*) the synthetic spectra are for $\log \varepsilon(\mathrm{Th}) = -\infty$, -3.08, -2.58, and -2.08. In each panel the synthetic spectrum drawn as a solid line represents the predicted total absorption without the presence of the Th II line, and the dotted lines represent varying amounts of additional thorium.

than that predicted for the canonical first dredge-up in such low-mass, low-metallicity stars. The extra mixing almost surely begins at the red giant stage in which the outwardly advancing H-burning shell contacts the molecular weight barrier left behind by the first dredge-up. Recent theoretical studies of this phenomenon have been conducted by Charbonnel (1994); new observational confirmation and references to prior work are given by Gratton et al. (1999).

Our stars match well the general trends of CNO abundances in low-metallicity giants. But the carbon abundance in HD 115444 relative to HD 122563 is large [$\Delta \log \varepsilon(\mathrm{C}) = +0.10$, compared to $\Delta \log \varepsilon(\mathrm{Fe}) = -0.24$]. Moreover, HD 122563 has a smaller isotopic ratio ($^{12}\mathrm{C}/^{13}\mathrm{C} \simeq 4$) than does HD 115444 ($^{12}\mathrm{C}/^{13}\mathrm{C} \simeq 6$), and it also has a smaller log ε(C). Therefore, one obvious possibility is that HD 122563, at a more advanced giant branch evolutionary state (lower T_{eff}, lower M_V) than HD 115444, has had a chance to mix more CN-cycle products to its surface. The C abundances with respect to iron are [C/Fe] = -0.11 for HD 115444, and [C/Fe] = -0.46 for HD 122563. Mean C abundances in low-metallicity giants average [C/Fe] ~ 0.0, but individual cases vary widely: some stars have [C/Fe] ~ -0.5, and others have extreme overabundances, [C/Fe] $\gtrsim +1.0$ (e.g., McWilliam et al. 1995; Norris et al. 1997a). The McWilliam et al. carbon abundances for stars with $-2.5 \geq$ [Fe/H] ≥ -3.0 naturally divide into low-carbon ($\langle$[C/Fe]$\rangle = -0.48 \pm 0.08$) and high-carbon ($\langle$[C/Fe]$\rangle = +0.14 \pm 0.06$) groups. The low-carbon group of six stars has $\langle \log g \rangle = 0.9 \pm 0.1$, and the high-carbon group of eight stars has $\langle \log g \rangle = 2.0 \pm 0.2$. Thus HD 115444 and HD 122563 seem to have [C/Fe] ratios consistent with their metallicities and gravities.

An alternative interpretation might link large carbon abundances with large neutron-capture abundances in UMP giants, because [C/Fe] = $+1.0$ in the extremely r-process–rich star CS 22892$-$052. In this view, the milder enhancement of the r-process abundances in HD 115444 has been accompanied by a much smaller carbon enhancement. To test this idea, we plotted the [Eu/Fe] ratios for a sample of 28 field halo giants (from Burris et al. 1999) against their [C/Fe] ratios (from Kraft et al. 1982). The result was a scatter diagram. Nor did a correlation emerge when newly derived [C/Fe] ratios for 27 of these stars (Rossi, Beers, & Sneden 1999) were correlated with the [Eu/Fe] values.

At present, differences in convective envelope dredge-up efficiency seems the more likely explanation for the difference in carbon abundance of our two stars. We would like to ascribe the slightly higher $^{12}\mathrm{C}/^{13}\mathrm{C}$ ratio of HD 115444 to this phenomenon also, but the observational uncertainties here are too large to support such a claim. Determination of nitrogen abundances for the McWilliam et al. (1995) sample could illuminate this question further. However, the observed [(C+N)/Fe] abundance sums for these stars are much larger than those that would be expected if they began their lives with [C/Fe] = [N/Fe] = 0.0 (as is observed in metal-poor main-sequence stars; see, e.g., Laird 1985; Carbon et al. 1987; Tomkin & Lambert 1984; Tomkin, Sneden, & Lambert 1986). This cannot be resolved until nitrogen abundance scale questions are satisfactorily understood.

The derived oxygen abundances, [O/Fe] $\simeq +0.6$, are among the largest reported values for metal-poor giants from analyses of the [O I] λ6300 line. Previous surveys of such stars (Gratton & Ortolani 1986; Barbuy 1988; Gratton et al. 1999) have found $\langle$[O/Fe]$\rangle \simeq +0.35$ for 25 stars in the metallicity range $-1.0 \geq$ [Fe/H] ≥ -2.5. Thus our larger [O/Fe] values may provide some support for the recent suggestions (Israelian, García Lopez, & Rebolo 1998; Boesgaard et al. 1999) that [O/Fe] increases with decreasing [Fe/H]. But the present study lacks appropriate control stars at higher metallicities; caution must be observed as systematic observational/analytical errors can produce shifts between different studies. This point should be pursued with uniform data sets of very high S/N spectra in future studies.

4.2. *Abundances of the Iron-Peak Elements*

Recall from Figure 5 that the relative abundances $\Delta \log \varepsilon$(X) of nearly all Fe-peak elements are mostly consistent with the relative iron abundance metallicity difference $\Delta \log \varepsilon$(Fe) between the two stars. Given this unity (based on eight elements), the relative manganese abundance $\Delta \log \varepsilon(\mathrm{Mn}) \simeq -0.5$ is quite different. Both stars are, however, within the range in [Mn/Fe] found for other stars of similar metallicity (see McWilliam et al. 1995). Nakamura et al. (1999) have suggested that variations in the mass cut in Type II supernova explosions could lead to low values of certain elements such as [Mn/Fe] in low-metallicity stars. A deeper mass cut would expel larger amounts of complete Si-burning products (i.e., Fe) but the same amount of incomplete Si-burning products (such as Mn), yielding net lower ratios of [Mn/Fe]. Such supernovae with deeper mass cuts would also presumably eject more neutron-rich (i.e., r-process) material consistent with the abundances in HD 115444. However, the Nakamura et al. results suggest that, for a deep supernova mass cut, not just Mn but also other products of incomplete Si burning, such as Cr, should show the same trend of low values with respect to Fe, while the products of complete Si burning, such as Co, should behave in the opposite manner. Our Cr and Co abundances do show such effects, but they are nearly identical in the two stars; the Cr and Co abundances do not indicate a mass-cut difference in supernova progenitors to HD 115444 and HD 122563. Thus, while the depth of the mass cut might suggest a possible correlation between low Mn and high r-process element abundances in HD 115444, either some further quantitative exploration of the Nakamura et al. ideas or an alternative explanation for the low Mn abundance might be required.

The mild relative overabundance of Ti in HD 115444, $\Delta \log \varepsilon(\mathrm{Ti}) = -0.06$, also does not seem to be predicted from inspection of the figures in Nakamura et al. (1999). The origin of this abundance difference may be due to differences in total (and/or core) masses of the probably relatively small sample of supernovae that once produced the heavy elements in the two stars. This suggestion is supported by recent early galactic nucleosynthesis simulations by Karlsson & Gustafsson (1999). Their models yield increasing scatter in [Ti/X], as well as in many other abundance ratios, as overall Fe metallicity decreases from [Fe/H] = -2.5 to [Fe/H] = -3.

4.3. *Abundances of the Neutron-Capture Elements*

The abundances of the elements Ba–Dy in HD 115444 are significantly larger ($\sim$10 times) than in HD 122563, even though the iron metallicity is very similar in these stars

(Table 4, Fig. 5). This gross difference between the absolute levels of the heaviest neutron-capture elements in these two stars is one more clear example that the abundances of the heavier elements vary greatly with respect to Fe in UMP stars of the early Galaxy (Gilroy et al. 1988; Burris et al. 1999). This presumably reflects the fact that the early Galaxy was not well mixed, with some stars receiving larger absolute amounts of neutron-capture material from individual nucleosynthetic events (almost certainly Type II supernovae).

Figure 8 shows the newly determined neutron-capture element abundances for HD 115444 along with the *HST* abundances of Sneden et al. (1998a). Superimposed upon the abundance data is the scaled solar system *r*-process elemental abundance distribution. The solar system *r*-process curve has been scaled vertically downward to account for the lower metallicity of this star with respect to the Sun. This elemental curve was obtained by summing over the isotopic abundances, and these were based on deconvolving the total solar system abundances (Anders & Grevesse 1989) into *s*- and *r*-process abundance fractions, using the neutron-capture cross sections of Käppeler et al. (1989) and Wisshak, Voss, & Käppeler (1996); see Sneden et al. (1996) and Burris et al. (1999) for details of this procedure.

The agreement between the heavier elements ($Z \geq 56$) and the scaled solar system curve is very striking in Figure 8. While there has been increasing evidence that this pattern is true for elements in the range $56 \leq Z \leq 70$, there have been few data for even heavier stable elements ($76 \leq Z \leq 83$, Os $\leftrightarrow$ Bi, also known as third *r*-process peak). The new observations of HD 115444 confirm the scaled solar system *r*-process pattern throughout the range $56 \leq Z \leq 78$. This in turn argues for a common site for *r*-process synthesis of these elements. Possible sites include supernovae and neutron star binaries; see Wheeler, Cowan, & Hillebrandt (1998) and Freiburghaus et al. (1999) for an extended theoretical discussion. But the observations will not easily support a wide range of allowable *r*-process parameters: a narrow range of progenitor star masses (e.g., Mathews, Bazan, & Cowan 1992; Wheeler et al. 1998) or a narrow range of nuclear and astrophysical conditions in the *r*-process sites (e.g., Freiburghaus et al. 1999) are required.

The lighter neutron-capture elements Ge, Sr, Y, and Zr shown in Figure 5 present a puzzle, as their abundances are very similar in the two stars. This suggests that the abundances of these elements are dependent upon metallicity, unlike the heavier elements (see also McWilliam et al. 1995; Sneden et al. 1998a; Burris et al. 1999; Cowan et al. 1999a). Moreover, these elements in both stars are poorly matched by the scaled solar system *r*-process curve in Figure 8. Further observational evidence supporting this point comes from the identification of several elements in the $41 \leq Z \leq 48$ range from new near-UV spectra of CS 22892−052 (Cowan et al. 1999b). The scaled solar system *r*-process curve is also not a good fit to the abundances of that more extensive set of elements with $Z < 56$. These mismatches might demonstrate the existence of such a "second *r*-process" that synthesizes these lighter *r*-process nuclei in a different environment than the heavier *r*-process nuclei (see Wasserburg, Busso, & Gallino 1996; Qian, Vogel, & Wasserburg 1998). More extensive theoretical abundance

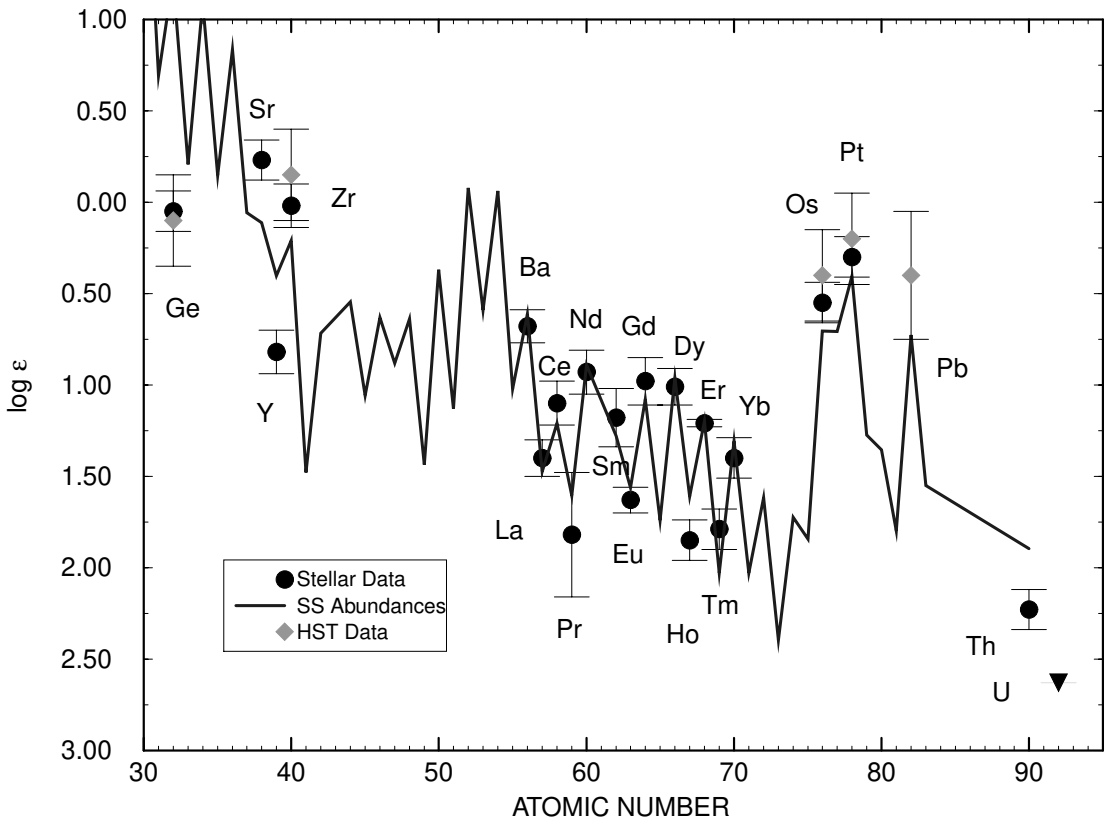

FIG. 8.—Neutron-capture abundances in HD 115444 (*filled circles*). *HST* abundances from Sneden et al. (1998) are indicated by filled diamonds, and for those elements the filled circles represent our reanalysis of the *HST* data. The line labeled "SS Abundances" in the figure is the scaled solar system *r*-process-only abundance curve. See the text for further explanation of the match to the solar system distribution.

predictions of these elements (see, e.g., Gallino et al. 1999) are clearly needed here.

We have made quantitative comparisons of the abundances of elements with $56 \leq Z \leq 78$ in HD 115444 and CS 22892−052 to the solar system *r*-process abundance distribution. Here these elements will be collectively referred to as "heavy-*r*" elements. The weighted mean abundance offset of the heavy-*r* elements for HD 115444 is $\langle$[heavy-*r*/H]$\rangle = -2.06 \pm 0.03$ ($\sigma = 0.10$; 14 elements), and for CS 22892−052 $\langle$[heavy-*r*/H]$\rangle = -1.44 \pm 0.02$ ($\sigma = 0.06$; 16 elements). In these calculations, the weight employed for each element's abundance was its observed line-to-line scatter standard deviation. However, weighting by the number of lines used, or assigning equal weights to each element, produced little change in the mean abundances. These means represent the *r*-process abundance levels of the heavy stable elements in the two stars. In the top and middle panels of Figure 9 we show the scatter about the means for HD 115444 and CS 22892−052. The larger scatter for HD 115444 seen in the top panel is evidence of the weaker absorption lines of neutron-capture species in this star compared to those of CS 22892−052, which increased the analysis difficulties for some elements. For example, the Tm abundance for HD 115444 comes from a single very weak and blended Tm II transition at 3700.2 Å, while in CS 22892−052 four Tm II lines were analyzed by Sneden et al. (1996). But in both stars it is clear that there is a single-valued abundance offset from the heavy-*r* solar system distribution.

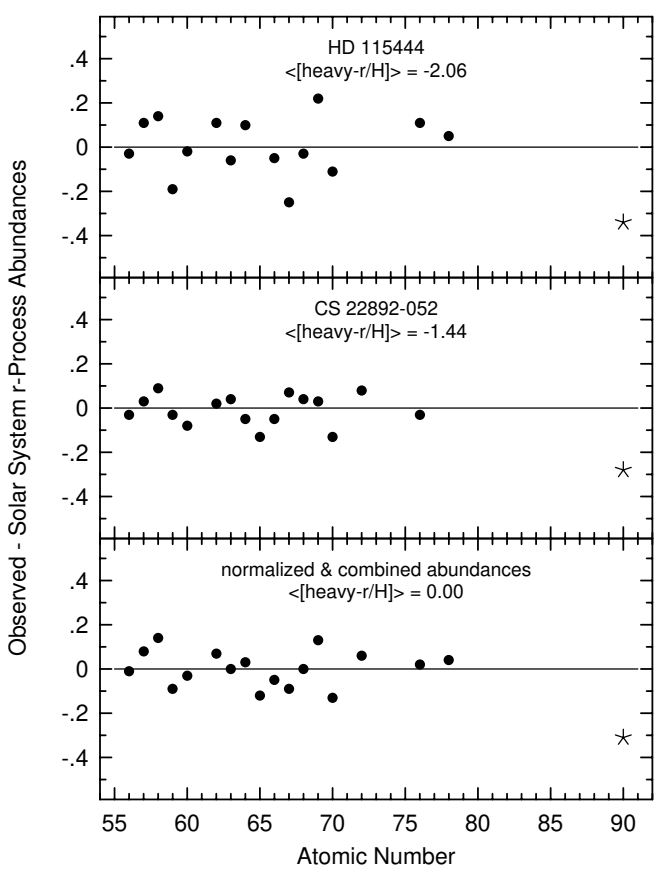

FIG. 9.—Differences between normalized observed abundances of elements with $Z \geq 56$ to *r*-process abundances of these elements in the solar system. See the text for explanations of the normalization constant indicated for the abundances displayed in each panel, and of the combination method for the abundances in the bottom panel. Derived abundances of stable elements in this atomic-number range are indicated by filled circles, and those of the radioactively unstable element thorium is indicated with five-pointed stars.

The bottom panel of Figure 9 shows the comparison of a combined abundance set (HD 115444 plus CS 22892−052) with the heavy-*r* solar system values. The combined stellar set was formed by first normalizing each star's heavy-*r* abundances by the mean abundance described above [$\log \varepsilon(\mathrm{X})_{\mathrm{HD}115444} + 2.06$ and $\log \varepsilon(\mathrm{X})_{\mathrm{CS}22892-052} + 1.44$]. Then we computed straight means of the normalized abundances for those elements analyzed in both stars, or else adopted the normalized abundances of one star when there was none available for the other star. Thus the abundance of terbium and hafnium in the combined set comes only from CS 22892−052, while the platinum abundance comes only from HD 115444. Comparing this normalized, combined data set to the solar system *r*-process distribution yielded $\langle$[heavy-*r*/H]$\rangle = 0.00 \pm 0.02$ ($\sigma = 0.08$; 17 elements). No element abundance in the combined data deviates by more than 0.13 dex from the solar system distribution. Figure 9 clearly demonstrates that the abundances of the heavy stable elements in HD 115444 and CS 22892−052 from $Z = 56$–78 are consistent with the solar system *r*-process abundances. While this has been suggested previously for CS 22892−052 (Sneden et al. 1996), we now have extensive neutron-capture element abundance data, including that in the third *r*-process peak, for two stars. These new data, particularly the normalized and combined abundances of HD 115444 and CS 22892−052 (as shown in Fig. 9) yield solid agreement with solar values, making other explanations for this abundance pattern (e.g., Goriely & Arnould 1997; Goriely & Clerbaux 1999) less likely. (See also further discussion in Freiburghaus et al. 1999.) As more *r*-process–rich UMP stars are discovered and subjected to detailed analysis, the accidental errors should decrease even further, leaving any remaining deviations to mark either true departures from the solar abundances or residual abundance analysis problems.

4.4. *Chronometers and Ages*

The detection of radioactive thorium in HD 115444 (Fig. 7) provides an opportunity to determine the radioactive age of this star. Consider first the chronometric age based solely on the HD 115444 abundances. To minimize errors in abundance determinations we have employed the ratio of thorium, produced solely in the *r*-process, to the stable abundance level of europium, an element overwhelmingly produced by the *r*-process (see Sneden et al. 1996; Burris et al. 1999). While Cowan et al. (1999a) found a preliminary value of $\log \varepsilon(\mathrm{Th}) = -2.1 \pm 0.07$ (based on an older model stellar atmosphere), our new synthesis indicates a value of $\log \varepsilon(\mathrm{Th}) = -2.23 \pm 0.07$, for thorium and an observed ratio of $\log \varepsilon(\mathrm{Th/Eu}) = -0.60$ in HD 115444. This value is very similar to that found previously for CS 22892−052, of $\log \varepsilon(\mathrm{Th/Eu}) = -0.66$ (Sneden et al. 1996).

The observed ratio of Th/Eu in HD 115444 can be compared to the initial predicted value at time of formation in an *r*-process environment. While the site for the *r*-process is still not well defined, abundances of the heaviest stable neutron-capture elements detected in HD 115444 and other stars can be used to constrain the predictions of theoretical *r*-process calculations. These same calculations can then be employed to predict the zero-decay age abundances of the

radioactive elements Th and U. Recently Pfeiffer, Kratz, & Thielemann (1997) and Cowan et al. (1999a), used the most massive stable solar isotopic abundances (i.e, ^{206,207,208}Pb and ^{209}Bi) to constrain the theoretical calculations. They conclude that the best fits to the observed solar data are obtained using the nuclear mass models FRDM-HFB (finite-range droplet with Hartree-Fock-Bogoliubov), the ETFSI-Q (extended Thomas-Fermi with Strutinsky integral and quenching) and the ETFSI-Q, lsq (least-squares fit applied to ETFSI-Q). These models predict initial values for Th/Eu of 0.496, 0.546, and 0.48, respectively (see Cowan et al. 1999a for details). Comparing these initial values with the observed stellar ratio yields values of 13.7, 15.7, and 13.1 Gyr, with an average age for HD 115444 of 14.2 Gyr.

We can make additional chronometric age determinations by also considering the case of CS 22892−052 and the mean abundances, as discussed in § 4.3 and shown in Figure 9. Not only do both stars have stable heavy *r*-process abundance distributions that are (within observational errors) identical with one another and with the solar system *r*-process distribution, but both stars show very similar and significantly subsolar abundances of thorium. This strongly implies that both stars are of similar age. For HD 115444, therefore, we can compute a ratio of Th to the mean abundance curve determined by all of the observed stable elements. Taking that value at $Z = 63$ (the position of Eu) suggests that the observed Eu value should be slightly higher by 0.05 in the log ϵ (comparable to our observational uncertainty), yielding a slightly different ratio of $\log (\mathrm{Th/Eu})_{\mathrm{mean}} = -0.65$. A similar exercise with the observed Eu abundance in CS 22892−052 suggests a similar correction in the opposite direction. Using the observed (Th and Eu) values from Sneden et al. (1996), we find a value of $\log (\mathrm{Th/Eu})_{\mathrm{mean}} = 0.61$, which agrees with the value for in HD 115444, again within the observational errors. Finally, the average of observed, corrected values for these two UMP stars [$\langle \log (\mathrm{Th/Eu})_{\mathrm{mean}} \rangle = -0.63$] yields the values reported by Cowan et al. (1999a): 15.2 (FRDM + HFB), 17.1 (ETFSI-Q) and 14.5 Gyr (ETFSI-Q, lsq), with a mean age of 15.6 Gyr for both stars.

With the detailed observations for two stars at this point, our analysis suggests a reduced (with respect to only one star) observational error in log ϵ of ± 0.05. Applying that abundance error to the mean age determination suggests age uncertainties of $(+2.3, -2.4)$ Gyr, based solely upon observational errors. Extensive error analysis and discussion (Cowan et al. 1999a) suggests that the calculations best fitting the solar data have typical theoretical uncertainties of ± 3 Gyr. If we assume an average observational uncertainty of 2.4 Gyr, then the total error (added in quadrature for uncorrelated errors) is approximately ± 4 Gyr, resulting in a final value of 15.6 ± 4 Gyr for the age of these two UMP stars.

These calculations demonstrate both the power and the sensitivity of this method, with small changes in observed values or theoretical predictions changing the ages by the order of several gigayears. While we have reduced the observational errors somewhat as a result of having two stars to analyze, it will be difficult to reduce the total error further without additional stellar observations of thorium and further theoretical calculations employing the most reliable mass formulae for nuclei far from stability. It is worth noting, however, that this radioactive-decay technique does not suffer from uncertainties in chemical evolution, since the timescale for such evolution in the early Galaxy is much shorter than the radioactive decay half-life (14 Gyr) of Th and the age of the Galaxy.

Additional supporting age information could be provided by the uranium chronometer in HD 115444, but we were only able to set an upper limit on the abundance of this element of $\log \varepsilon(\mathrm{U}) \leq -2.6$. Here is an age estimation based upon that upper limit. In contrast to the case for Th, in the case of U we have to take into account the two different isotopes, with very different half-lives, that make up this element. Theoretical calculations based upon the ETFSI-Q model (see Cowan et al. 1999a; Pfeiffer et al. 1997) predict that the initial U elemental abundance is dominated by the shorter half-life isotope, ^{235}U, while presumably the elemental abundance in the metal-poor stars is mostly determined by ^{238}U. Ignoring the initial ^{235}U production entirely (this isotope decays in much less than a Hubble time), and only comparing the initial time-zero ^{238}U and the observed upper limit in HD 115444, gives a lower limit on the age of this star of more than 11 Gyr. This value is already within the estimated error for the Th age estimate. Since the actual U abundance may be much below our upper limit, the implied lower limit on the stellar age (based upon the nondetection of U) is in reasonable accord with the Th age determination.

The thorium age estimates determined here, both for HD 115444 by itself and by considering both UMP stars, are consistent with our earlier age estimates for CS 22892−052, the (so far) only other metal-poor Galactic halo star for which abundances of Th and an extensive set of other neutron-capture elements have been determined (Cowan et al. 1997, 1999a; Pfeiffer et al. 1997). Further, these new chronometric age determinations agree well with recent globular cluster age estimates (see Pont et al. 1998) and cosmological age determinations of 14.9 ± 1.5 Gyr (Perlmutter et al. 1999) and 14.2 ± 1.7 Gyr (Riess et al. 1998). While values of the Hubble constant near 70 km s^{-1} Mpc^{-1} and a flat universe would imply cosmological age estimates much less than this, most recent work has suggested a relatively low-density universe, which along with that Hubble constant have suggested a corresponding universal age of 13 Gyr (see, e.g., Freedman 1999), still consistent with our estimated stellar chronometric ages. We note, however, that we have found thorium in only two stars so far, and additional detections will be needed to strengthen this technique of radioactive dating.

5. CONCLUSIONS

We have performed a detailed abundance analysis of the UMP field giant HD 115444. In addition to treating HD 115444 alone in a standard model atmosphere analysis of equivalent widths and synthetic spectra, we have made a line-by-line abundance comparison with the well-known UMP giant HD 122563. The differential study yields very accurate relative atmosphere parameters and abundances that illuminate a number of similarities and sharp disagreements in the chemical compositions of these two stars. Here we summarize the main results, which confirm and greatly extend the initial spectroscopic investigations by GGGV82 and Gilroy et al. (1988).

1. HD 115444's mean Fe-peak metallicity is approximately 0.24 dex lower than that of HD 122563. It is a slightly less evolved star, with $\Delta T_{\mathrm{eff}} \simeq +150$ K, $\Delta \log g \simeq +0.2$, and $\Delta M_V \simeq +0.6$. The absolute metal-

licity of HD 115444 is [Fe/H] = −2.99, in good agreement with GGGV82, but this number is somewhat dependent on the adopted temperature scale, choice of model atmosphere, and assumptions made in constructing the models.

2. For elements with $Z \leq 30$, HD 115444 has a fairly typical halo star abundance distribution. But comparison with HD 122563 reveals several significant differences in abundance patterns. Most notable are the large relative overabundance of carbon and underabundance of manganese in HD 115444, and the smaller but significant overabundance of titanium.

3. The lighter neutron-capture elements ($32 \leq Z \leq 40$) are only mildly enhanced in HD 115444; the mean relative overabundance is $\langle \Delta[\text{Ge, Sr, Y, Zr/Fe}] \rangle = +0.18$ compared to HD 122563.

4. The heavier neutron-capture elements ($Z \geq 56$) in HD 115444 are very enhanced: $\langle \Delta[\text{Ba, La, Nd, Eu, Er, Yb/Fe}] \rangle = +0.95$. The abundance pattern among these elements is consistent with a scaled solar system *r*-process distribution.

5. Thorium is underabundant relative to the other heavy neutron-capture elements, as it is in CS 22892−052. A simple age estimate for these two stars is 15.6 ± 4 Gyr.

We thank Roberto Gallino, Inese Ivans, Francesca Primas, Friedel Thielemann, Jim Truran, Craig Wheeler, and referee Roger Cayrel for helpful discussions and comments on this paper. Model atmospheres used in this paper were kindly computed by Bengt Edvardsson. J. W. is grateful for financial support from the international student exchange program between Uppsala University and the University of Texas. This research was funded in part by NSF grants AST 96-18364 to C. S. and AST 96-18332 to J. J. C. Additional support was provided through grants GO-05421, GO-05856, and GO-06748 from the Space Science Telescope Institute, which is operated by the Association of Universities for Research in Astronomy, Inc., under NASA contract NAS 5-26555.

REFERENCES

Alonso, A., Arribas, S., & Martínez-Roger 1998, A&AS, 131, 209
Anders, E., & Grevesse, N. 1989, Geochim. Cosmochim. Acta, 53, 197
Anthony-Twarog, B. J., & Twarog, B. A. 1994, AJ, 107, 1577
Arpigny, C., & Magain, P. 1983, A&A, 127, L7
Barbuy, B. 1988, A&A, 191, 121
Beers, T. C., Preston, G. W., & Shectman, S. A. 1985, AJ, 90, 2089
———. 1992, AJ, 103, 1987
Boesgaard, A. M., King, J. R., Deliyannis, C. P., & Vogt, S. S. 1999, AJ, 117, 492
Bond, H. E. 1980, ApJS, 44, 517
Burris, D. L., Pilachowski, C. A., Armandroff, T., Sneden, C., Roe, H., & Cowan, J. J. 1999, ApJ, submitted
Butcher, H. R. 1987, Nature, 328, 127
Carbon, D. F., Barbuy, B., Kraft, R. P., Friel, E. D., & Suntzeff, N. B. 1987, PASP, 99, 335
Cayrel, R. 1996, A&A Rev., 7, 217
Cayrel de Strobel, G., Soubiran, C., Friel, E. D., Ralite, N., & François, P. 1997, A&AS, 125, 299
Charbonnel, C. 1994, A&A, 282, 811
Clariá, J. J., Minniti, D., Piatti, A. E., & LaPasset, E. 1994, MNRAS, 268, 733
Cowan, J. J., Burris, D. L., Sneden, C., Preston, G. W., & McWilliam, A. 1995, ApJ, 439, L51
Cowan, J. J., McWilliam, A., Sneden, C., Burris, D. L., & Preston, G. W. 1997, ApJ, 480, 246
Cowan, J. J., Pfeiffer, B., Kratz, K.-L., Thielemann, F.-K., Sneden, C., Burles, S., Tytler, D., & Beers, T. C. 1999a, ApJ, 521, 194
Cowan, J. J., Sneden, C., Ivans, I., Burles, S., Beers, T. C., & Fuller, G. 1999b, BAAS, 194, 67.04
Di Benedetto, G. P. 1998, A&A, 339, 858
Edvardsson, B., Andersen, J., Gustafsson, B., Lambert, D. L., Nissen, P. E., & Tomkin, J. 1993, A&A, 275, 101
ESA 1997, The *Hipparcos* Catalogue (ESA SP-1200; Paris: ESA)
Fitzpatrick, M. J., & Sneden, C. 1987, BAAS, 19, 1129
François, P., Spite, M., & Spite, F. 1993, A&A, 274, 821
Freedman, W. 1999, preprint (astro-ph/9905222)
Freiburghaus, C., Rembges, J.-F., Rauscher, T., Kolbe, E., Thielemann, F.-K., Kratz, K.-L., Pfeiffer, B., & Cowan, J. J. 1999, ApJ, 516, 381
Fuhr, J. R., & Wiese, W. L. 1996, NIST Atomic Transition Probability Tables, in Chemical Rubber Company Handbook of Chemistry and Physics, ed. D. R. Lide (Boca Raton: CRC), 10-128
Gallino, R., Busso, M., Lugaro, M., Travaglio, C., Arlandini, C., & Vaglio, P. 1999, in Nuclei in the Cosmos V, ed. N. Prantzos & S. Harissopulos (Paris: Editions Frontières), 216
Gilroy, K. K., Sneden, C., Pilachowski, C. A., & Cowan, J. J. 1988, ApJ, 327, 29
Goriely, S., & Arnould, M. 1997, A&A, 322, L29
Goriely, S., & Clerbaux, B. 1999, A&A, 346, 798
Gratton, R. G., & Ortolani, S. 1984, A&A, 137, 6
———. 1986, A&A, 169, 201
Gratton, R. G., & Sneden, C. 1990, A&AS, 86, 269
Gratton, R. G., Sneden, C., Carretta, E., & Bragaglia, A. 1999, A&A, submitted
Griffin, R. F. 1967, ApJ, 148, 465
Griffin, R., Griffin, R., Gustafsson, B., & Vieira, T. 1982, MNRAS, 198, 637 (GGGV82)
Gustafsson, B., Bell, R. A., Eriksson, K., & Nordlund, Å. 1975, A&A, 42, 407
Hanson, R. B., Sneden, C., Kraft, R. P., & Fulbright, J. 1998, AJ, 115, 1500
Henyey, L., Vardya, M. S., & Bodenheimer, P. 1965, ApJ, 142, 841
Israelian, G., García Lopez, R. J., & Rebolo, R. 1998, ApJ, 507, 805
Käppeler, F., Beer, H., & Wisshak, K. 1989, Rep. Prog. Phys., 52, 945
Karlsson, T., & Gustafsson, B. 1999, in Proc. 35th Liège International Astrophysics Colloq., The Galactic Halo: From Globular Clusters to Field Stars, in press
Kraft, R., Suntzeff, N., Langer, G., Carbon, D., Trefzger, C., Friel, E., & Stone, R. 1982, PASP, 94, 55
Kurucz, R. L. 1999, http://cfaku5.harvard.edu
Laird, J. B. 1985, ApJ, 289, 556
Lambert, D. L., & Sneden, C. 1977, ApJ, 215, 591
Lambert, D. L., Sneden, C., & Ries, L. M. 1974, ApJ, 188, 97
Mathews, G. J., Bazan, G., & Cowan, J. J. 1992, ApJ, 391, 719
McWilliam, A. 1998, AJ, 115, 1640
McWilliam, A., Preston, G. W., Sneden, C., & Searle, L. 1995, AJ, 109, 2736
Montegriffo, P., Ferraro, F. R., Origlia, L., & Fusi Pecci, F. 1998, MNRAS, 297, 872
Morell, O., Källander, D., & Butcher, H. R. 1992, A&A, 259, 543
Nakamura, T., Umeda, H., Nomoto, K., Thielemann, F.-K., & Burrows, A. 1999, ApJ, 517, 193
Norris, J. E., Ryan, S. G., & Beers, T. C. 1997a, ApJ, 488, 350
———. 1997b, ApJ, 489, L169
Perlmutter, S., et al. 1999, ApJ, 517, 565
Pfeiffer, B., Kratz, K.-L., & Thielemann, F.-K. 1997, Z. Phys. A, 357, 235
Pilachowski, C. A., Sneden, C., & Kraft, R. P. 1996, AJ, 111, 1689
Pont, F., Mayor, M., Turon, C., & VandenBerg, D. A. 1998, A&A, 329, 87
Qian, Y.-Z., Vogel, P., & Wasserburg, G. J. 1998, ApJ, 506, 868
Riess, A. G., et al. 1998, AJ, 116, 1009
Rossi, S., Beers, T. C., & Sneden, C. 1999, in ASP Conf. Ser. 165, The Third Stromlo Symposium; The Galactic Halo, ed. B. K. Gibson, T. S. Axelrod, & M. E. Putman, 165, 264
Ryan, S. G., Norris, J. E., & Beers, T. C. 1996, ApJ, 471, 254
Sneden, C. 1973, ApJ, 184, 839
Sneden, C., Cowan, J. J., Burris, D. L., & Truran, J. W. 1998a, ApJ, 496, 235
Sneden, C., Fuller, G. M., Burles, S., Beers, T. C., & Cowan, J. J. 1998b, BAAS, 193, 45.12
Sneden, C., Gratton, R. G., & Crocker, D. A. 1991, A&A, 246, 354
Sneden, C., McWilliam, A., Preston, G. W., Cowan, J. J., Burris, D. L., & Armosky, B. J. 1996, ApJ, 467, 819
Sneden, C., & Parthasarathy, M. 1983, ApJ, 267, 757
Sneden, C., Pilachowski, C. A., & VandenBerg, D. A. 1986, ApJ, 311, 826
Sneden, C., Preston, G. W., McWilliam, A., & Searle, L. 1994, ApJ, 431, L27
Tomkin, J., & Lambert, D. L. 1984, ApJ, 279, 220
Tomkin, J., Sneden, C., & Lambert, D. L. 1986, ApJ, 302, 415
Tull, R. G., MacQueen, P. J., Sneden, C., & Lambert, D. L. 1995, PASP, 107, 251
Wasserburg, G. J., Busso, M., & Gallino, R. 1996, ApJ, 466, 109
Wheeler, J. C., Cowan, J. J., & Hillebrandt, W. 1998, ApJ, 493, L101
Wisshak, K., Voss, F., & Käppeler, F. 1996, in Proc. 8th Workshop on Nuclear Astrophysics, ed. W. Hillebrandt & E. Müller (Munich: MPI), 16